This is a preprint of an article accepted for publication in Journal of Applied Mathematical Modelling on 29 April 2014. The published article is available online at http://www.sciencedirect.com/science/article/pii/S0307904X14002418
To be cited as: Bouaanani N., Miquel B. 2015. Efficient modal dynamic analysis of flexible beam-fluid systems. Journal of Applied Mathematical Modelling, 1: 99–116.

Efficient Modal Dynamic Analysis of Flexible Beam-Fluid Systems

Najib Bouaanani [1] and Benjamin Miquel [2]

ABSTRACT

This paper proposes an efficient simplified method to determine the modal dynamic and earthquake response of coupled flexible beam-fluid systems and to evaluate their natural vibration frequencies. The methodology developed extends available analytical solutions for mode shapes and natural vibration frequencies of slender beams with various boundary conditions to include the effects of fluid-structure interaction. The proposed method is developed for various beam boundary conditions considering lateral interaction with one or two semi-infinite fluid domains. Numerical examples are provided to illustrate the application of the proposed method, and the obtained results confirm the importance of accounting for fluid-structure interaction effects. We show that the developed procedure yields excellent results when compared to more advanced coupled fluid-structure finite element solutions, independently of the number of included modes, beam boundary conditions, and number of interacting fluid domains. The proposed simplified method can be easily implemented in day-to-day engineering practice, as it constitutes an efficient alternative solution considering the fluid-structure modeling complexities and related high expertise generally involved when using advanced finite elements.

Key words: Dynamic and seismic effects; Beam-fluid systems; Natural frequencies; Simplified methods; Fluid-Structure interaction; Finite elements.

[1] Professor, Department of Civil, Geological and Mining Engineering, Polytechnique Montréal, Montréal, QC H3C 3A7, Canada.
Corresponding author. E-mail: najib.bouaanani@polymtl.ca
[2] Graduate Research Assistant, Department of Civil, Geological and Mining Engineering, Polytechnique Montréal, Montréal, QC H3C 3A7, Canada.

1 Introduction

Several civil engineering and industrial applications involve the vibrations of beam-like structures in contact with water or fluid domains, including dams, navigation locks, quay walls, break-waters, offshore platforms, drilling risers, liquid storages, nuclear reactors, oil refineries, petrochemical plants, fuel storage racks, etc. This popular topic has attracted many researchers over the last decades and various approaches were proposed, varying from simplified to more complex analytical and numerical formulations. Neglecting structural flexibility, Westergaard [1] introduced the added-mass concept and applied it to a dam-reservoir system, and later Jacobsen [2] and Rao [3] generalized the added-mass formulation to evaluate hydrodynamic effects on rigid circular and rectangular piers vibrating in water. Goto and Toki [4] and Kotsubo [5] evaluated the hydrodynamic pressures induced by harmonic motions on circular or elliptical cross-section cylindrical towers along rigid body and deformed mode shapes. Chopra [6, 7] showed that a dam's flexibility influences significantly its interaction with the impounded reservoir, and consequently the overall dynamic and seismic responses. Other studies also confirmed the importance of accounting for structural flexibility and fluid-structure interaction [8–11]. Han and Xu [12] developed an analytical model to compute the modal properties of a slender flexible cylinder vibrating in water, and proposed a simplified added-mass formula to compute its natural frequencies. Other researchers studied the sensitivity of the hydrodynamic response of cantilever structures to various factors, such as: (i) a tip mass or inertia concentrated at one end [13–16], (ii) a restrained boundary condition at the base of the beam [16–18], and (iii) non-uniformity of beam cross-section [16, 17, 19].

Most of the previous studies focused on cantilever structures surrounded by fluid. Work on beam-like structures interacting with 2D semi-infinite fluid domains was mainly related to dam monoliths impounding water reservoirs, while fewer researchers investigated the behavior of slender beams subjected to hydrodynamic loading of the latter type. Xing et al. [20], Zhao et al. [21] and Xing [22] developed analytical formulations to examine the dynamic response of a cantilever flexible beam interacting with a 2D semi-infinite water domain, and discussed the effects of various boundary conditions of the fluid domain. Nasserzare et al. [23] proposed a procedure to extract the natural frequencies and modes of a dry structure from vibrational data containing fluid-structure interaction effects, and they applied the methodology to a beam-water system. De Souza and Pedroso [24] developed a finite element procedure to determine the coupled dynamic response of a Bernoulli beam interacting with a 2D acoustical cavity, and they validated the vibration frequencies and modes obtained by comparing to other finite element and analytical solutions.

The present paper is motivated by the need to develop simplified methods extending results from classical vibration beam theory to include the effects of 2D hydrodynamic forces on one or both sides of a vibrating beam. The majority of the previous work and other relevant literature addressed hydrodynamic effects on cantilever beams, fully clamped or partially

restrained at the base, and little attention has been given to other boundary conditions such as pinned or sliding supports. Most of the previous studies also focused on the determination of the modal properties of a vibrating beam interacting with a fluid, while less concern has been devoted to the time evolution of beam's earthquake response indexes such as displacements, shear forces, and bending moments. These restrictions will be addressed in this paper.

2 Modal dynamic response of a beam-fluid system

2.1 Basic assumptions and notation

Fig. 1 shows a slender beam of height H vibrating in contact with fluid on one or both sides. We adopt a Cartesian coordinate system with origin at the base of the beam, a horizontal axis x and a vertical axis y coincident with the axis of symmetry of the beam. The semi-infinite fluid domains have a rectangular geometry with constant height equal to that of the beam. We denote by Λ_{f} the number of fluid domains in contact with the beam, and by left and right side fluid domains those extending from the beam towards negative and positive x directions, respectively. Both configurations illustrated in Figs. 1 (a) and (b) will be investigated here, i.e. $\Lambda_{\mathrm{f}}=1$ and $\Lambda_{\mathrm{f}}=2$, respectively. The beam will be referred to as dry when it is in contact with one fluid domain at least, i.e. $\Lambda_{\mathrm{f}}>0$, and wet otherwise. The boundary conditions of the beam can be Clamped-Free (CF) as shown in Fig. 1 or Clamped-Pinned (CP), Clamped-Sliding (CS), Clamped-Clamped (CC) or Pinned-Pinned (PP) as illustrated in Fig. 2. Points at the top, middle and base of the beam are denoted by A, B and C, respectively, as shown in Fig. 1 (a). These points will be used later to illustrate various dynamic responses of the studied beams. We also assume that: (i) the beam is slender so that only flexural deformations are considered, i.e. Euler-Benoulli beam theory is used; (ii) the beam is made of a linear, homogenous, and isotropic elastic material; (iii) only small deflections normal to the undeformed beam axis are included; (iv) the fluid is incompressible and inviscid, with its motion irrotational and limited to small amplitudes, (v) the fluid remains in full contact with the beam during vibration due to the assumption of small displacements, and (vi) gravity surface waves and non-convective effects are neglected.

2.2 Governing equations

We first assume that the beam-fluid system is subjected to a unit harmonic free-field horizontal ground motion $\ddot{u}_{\mathrm{g}}(t)=\mathrm{e}^{\mathrm{i}\omega t}$, where ω denotes a forcing frequency, t the time variable and i the unit imaginary number. Using a modal superposition analysis, the frequency response functions along beam's height of lateral displacement u, lateral acceleration $\ddot{u}$, bending mo-

ment $\mathcal{M}$ and shear force $\mathcal{V}$ can be expressed as

$$\bar{u}(y,\omega) = \sum_{j=1}^{N_\mathrm{s}} \psi_j(y)\,\bar{Z}_j(\omega)\,; \qquad \bar{\ddot{u}}(y,\omega) = -\omega^2 \sum_{j=1}^{N_\mathrm{s}} \psi_j(y)\,\bar{Z}_j(\omega) \tag{1}$$

$$\bar{\mathcal{M}}(y,\omega) = EI \sum_{j=1}^{N_\mathrm{s}} \bar{Z}_j(\omega) \frac{\partial^2 \psi_j(y)}{\partial y^2}\,; \qquad \bar{\mathcal{V}}(y,\omega) = EI \sum_{j=1}^{N_\mathrm{s}} \bar{Z}_j(\omega) \frac{\partial^3 \psi_j(y)}{\partial y^3} \tag{2}$$

where N_s denotes the number of dry beam modes included in the analysis, ψ_j the x–component of the $j^{\,\mathrm{th}}$ vibration mode shape $\boldsymbol{\psi}_j$, $j = 1 \ldots N_\mathrm{s}$, of the dry beam, $\bar{Z}_j$ the corresponding generalized coordinate, E the modulus of elasticity of the beam and I the moment of inertia of the beam about bending neutral axis.

Based on previous studies [25–27], the vector $\bar{\mathbf{Z}}$ of generalized coordinates $\bar{Z}_j(\omega)$, $j = 1 \ldots N_\mathrm{s}$, can be obtained by solving the system of equations

$$\bar{\mathbf{S}}\,\bar{\mathbf{Z}} = \bar{\mathbf{Q}} \tag{3}$$

which translates the beam-fluid system's dynamic equilibrium between inertia, damping and elastic forces resulting from the vibrations of the beam and hydrodynamic forces generated by the interacting fluid domain(s). The elements of matrix $\bar{\mathbf{S}}$ and vector $\bar{\mathbf{Q}}$ in Eq. (3) are obtained for $j = 1 \ldots N_\mathrm{s}$ and $m = 1 \ldots N_\mathrm{s}$ as

$$\bar{S}_{j,m}(\omega) = \left[-\omega^2 + (1 + \mathrm{i}\,\eta)\,\omega_j^2 \right] M_j\,\delta_{j,m} - \Lambda_\mathrm{f}\,\omega^2 \int_0^H \bar{p}_j(y,\omega)\,\psi_m(y)\,\mathrm{d}y \tag{4}$$

and

$$\bar{Q}_m = -L_m - \Lambda_\mathrm{f} \int_0^H \bar{p}_0(y,\omega)\,\psi_m(y)\,\mathrm{d}y \tag{5}$$

in which $\delta_{j,m}$ denotes the Kronecker symbol and

- $\bar{p}_0$ is the frequency response function for hydrodynamic pressure exerted on the left side of the beam due to its rigid body motion;
- $\bar{p}_j$ is the frequency response function for hydrodynamic pressure exerted on the left side of the beam due to its horizontal acceleration $\psi_j(y)$;
- ω_j is the natural frequency corresponding to the $j^{\,\mathrm{th}}$ dry beam vibration mode shape $\boldsymbol{\psi}_j$;
- η is an assumed constant hysteretic damping ratio;
- M_j and L_m are respectively the generalized mass and force given by

$$M_j = \mu_\mathrm{s} \int_0^H \left[\psi_j(y)\right]^2 \mathrm{d}y = \mu_\mathrm{s}\,H \int_0^1 \left[\bar{\psi}_j(\bar{y})\right]^2 \mathrm{d}\bar{y} = \mu_\mathrm{s}\,H\,M_j^* \tag{6}$$

$$L_m = \mu_\mathrm{s} \int_0^H \psi_m(y)\,\mathrm{d}y = \mu_\mathrm{s}\,H \int_0^1 \bar{\psi}_m(\bar{y})\,\mathrm{d}\bar{y} = \mu_\mathrm{s}\,H\,L_m^* \tag{7}$$

  in which μ_s is the beam's mass per unit height and $\bar{\psi}$ is a function resulting from the introduction of the change of variable $\bar{y} = y/H$ into the mode shape function ψ_j.

The mode shapes for slender beams were reported in many references such as [28–31]. The formulation given by Young and Felgar [28] and Blevins [30] is adopted here. The expressions of beam mode shapes are reviewed in Appendix A for the studied beam boundary conditions illustrated in Fig. 2. For each beam configuration, the expressions for parameters β_j and σ_j, $j = 1 \ldots N_\mathrm{s}$, required to obtain beam mode shapes are provided in Table A1. These parameters are computed using high precision arithmetic for the first 10 beam modes, i.e. $N_\mathrm{s} = 10$, and are given in Tables 1 to 7 for all the beam configurations studied. We note that high precision arithmetic is generally required to compute dry beam modes due to round off errors associated with the hyperbolic functions when the argument is large. This problem has been discussed by several authors such as in [29, 31].

Introducing beam mode shapes into the integrals of Eqs. (6) and (7), we show that: (i) the parameter $M_j^* = 1$, $j = 1 \ldots n$, for all beam boundary conditions except the PP beam configuration which corresponds to $M_j^* = 1/2$, $j = 1 \ldots n$, and (ii) that the parameter L_m^* can be evaluated for $m = 1 \ldots N_\mathrm{s}$ using the closed-form expressions

$$L_m^* = \frac{2\sigma_m}{\beta_m} \tag{8}$$

for CF and CS boundary conditions,

$$L_m^* = \frac{2\sigma_m}{\beta_m} \left[1 - \frac{\sinh(\beta_m)\, \sin(\beta_m)}{\cosh(\beta_m) - \cos(\beta_m)} \right] \tag{9}$$

for CP, PC and CC boundary conditions, and

$$L_m^* = -\frac{(-1)^m - 1}{m\pi} \tag{10}$$

for PP boundary conditions. Since the generalized mass parameter M_j^* is independent of the mode number j, the subscript j can be omitted for simplicity and Eq. (6) can be rewritten as

$$M = \mu_\mathrm{s}\, H\, M^* \tag{11}$$

for all the modes $j = 1 \ldots N_\mathrm{s}$.

The numerical values of parameters M^* and L_j^*, $j = 1 \ldots 10$, are given in Tables 1 to 7 for the studied beam configurations. Performing a change of integration variable as in Eqs. (6) and (7), and expressing hydrodynamic pressures as in [26, 27], we show that the integrals in Eqs. (4) and (5), which represent the effects of beam-fluid dynamic interaction, can be

expressed as the sum of N_f terms corresponding each to a mode n of the fluid domain

$$\int_0^H \bar{p}_j(y)\,\psi_j(y)\,\mathrm{d}y = \frac{4\rho_\mathrm{f}}{\pi}\,H^2 \sum_{n=1}^{N_\mathrm{f}} \frac{(I_{j,n})^2}{(2n-1)} = \frac{4\rho_\mathrm{f}}{\pi}\,H^2\,\theta^*_{j,j} \tag{12}$$

$$\int_0^H \bar{p}_j(y)\,\psi_m(y)\,\mathrm{d}y = \frac{4\rho_\mathrm{f}}{\pi}\,H^2 \sum_{n=1}^{N_\mathrm{f}} \frac{I_{j,n}\,I_{m,n}}{(2n-1)} = \frac{4\rho_\mathrm{f}}{\pi}\,H^2\,\theta^*_{j,m} \tag{13}$$

$$\int_0^H \bar{p}_0(y)\,\psi_m(y)\,\mathrm{d}y = -\frac{8\rho_\mathrm{f}}{\pi^2}\,H^2 \sum_{n=1}^{N_\mathrm{f}} \frac{(-1)^n I_{m,n}}{(2n-1)^2} = -\frac{8\rho_\mathrm{f}}{\pi^2}\,H^2\,\Gamma^*_m \tag{14}$$

where ρ_f denotes the fluid mass density, and the parameters $I_{\ell,n}$ are given for $\ell = 1 \ldots N_\mathrm{s}$ and $n = 1 \ldots N_\mathrm{f}$ as

$$I_{\ell,n} = \int_0^1 \bar{\psi}_\ell(\bar{y})\,\cos\left[\frac{(2n-1)\,\pi}{2}\,\bar{y}\right]\,\mathrm{d}\bar{y} \tag{15}$$

The integral in Eq. (15) can be evaluated using integration by parts, yielding the closed-form expressions

$$\begin{aligned} I_{\ell,n} =& (-1)^{n+1} \times 2\pi(2n-1)\left[\frac{\cosh(\beta_\ell)}{P_{\ell,n}} + \frac{\cos(\beta_\ell)}{R_{\ell,n}}\right] \\ &+ 2\sigma_\ell \times (-1)^n \times \pi(2n-1)\left[\frac{\sinh(\beta_\ell)}{P_{\ell,n}} + \frac{\sin(\beta_\ell)}{R_{\ell,n}}\right] + 4\sigma_\ell\,\beta_\ell\left[\frac{1}{P_{\ell,n}} + \frac{1}{R_{\ell,n}}\right] \end{aligned} \tag{16}$$

for beam configurations CF, CP, CS and CC,

$$\begin{aligned} I_{\ell,n} =& (-1)^{n+1} \times 2\pi(2n-1)\left[\frac{1}{P_{\ell,n}} + \frac{1}{R_{\ell,n}}\right] \\ &+ 4\beta_\ell\left[\frac{\sinh(\beta_\ell)}{P_{\ell,n}} - \frac{\sin(\beta_\ell)}{R_{\ell,n}}\right] - 4\sigma_\ell\,\beta_\ell\left[\frac{\cosh(\beta_\ell)}{P_{\ell,n}} + \frac{\cos(\beta_\ell)}{R_{\ell,n}}\right] \end{aligned} \tag{17}$$

for beam configurations PC and SC, and

$$I_{\ell,n} = \frac{4\beta_\ell}{R_{\ell,n}} \tag{18}$$

for beam configuration PP. The functions $P_{\ell,n}$ and $R_{\ell,n}$ in Eqs. (16) to (18) are defined by

$$P_{\ell,n} = 4\beta_\ell^2 + \pi^2\,[4n(n-1)+1]\;; \qquad\qquad R_{\ell,n} = 4\beta_\ell^2 - \pi^2(2n-1)^2 \tag{19}$$

for $\ell = 1 \ldots N_\mathrm{s}$ and $n = 1 \ldots N_\mathrm{f}$.

The expressions in Eqs. (16) to (18) show that the integrals in Eqs. (12) to (14) and corresponding series are convergent. For each studied beam configuration, the numerical values of parameters $\theta^*_{j,m}$ defined in Eqs. (12) to (14) are given in Tables 1 to 7 for $j = 1 \ldots 10$ and $m = 1 \ldots 10$. We note that high precision arithmetic was used to compute these parameters for maximum accuracy of the results [32]. Using the relations in Eqs. (12) to (14), it follows

that Eqs. (4) and (5) can be rewritten under a more compact form as

$$\bar{S}_{j,m}(\omega) = \Big[-\omega^2 + (1+\mathrm{i}\,\eta)\,\omega_j^2 \Big]\,\mu_\mathrm{s}\,H\,M^*\,\delta_{j,m} - \frac{4\rho_\mathrm{f}}{\pi}\,\Lambda_\mathrm{f}\,\omega^2\,H^2\,\theta^*_{j,m} \tag{20}$$

$$\bar{Q}_m = -\mu_\mathrm{s}\,H\,L^*_m + \frac{8\rho_\mathrm{f}}{\pi^2}\,\Lambda_\mathrm{f}\,H^2\,\Gamma^*_m \tag{21}$$

The natural frequencies ω_j in Eq. (20) can be obtained as [28, 30]

$$\omega_j = \alpha\,\beta_j^2 \qquad \text{for } j = 1 \ldots N_\mathrm{s} \tag{22}$$

where the parameter α is defined as

$$\alpha = \frac{1}{H^2}\sqrt{\frac{EI}{\mu_\mathrm{s}}} \tag{23}$$

2.3 Frequency and time domain response solutions

To obtain the dynamic frequency response of the studied beam-fluid systems, the system of equations (3) has first to be solved for the vector $\bar{\mathbf{Z}}$ of generalized coordinates considering frequencies ω in the range of interest. Standard matrix analysis numerical schemes could be used for that purpose. Once the generalized coordinates $\bar{Z}_j(\omega)$, $j = 1 \ldots N_\mathrm{s}$, are determined, frequency domain responses along beam's height of lateral displacement u, lateral acceleration $\ddot{u}$, bending moment $\mathcal{M}$ and shear force $\mathcal{V}$ can be determined using Eqs. (1) and (2). The corresponding time-history responses of the beam under the effect of an arbitrary ground acceleration $\ddot{u}_\mathrm{g}(t)$ of duration t_a, i.e. $0 \leqslant t \leqslant t_a$, are given by

$$u(y,t) = \sum_{j=1}^{N_\mathrm{s}} \psi_j(y)\,Z_j(t)\,; \qquad \ddot{u}(y,t) = \sum_{j=1}^{N_\mathrm{s}} \psi_j(y)\,\ddot{Z}_j(t) \tag{24}$$

$$\mathcal{M}(y,t) = EI\sum_{j=1}^{N_\mathrm{s}} Z_j(t)\frac{\partial^2\psi_j(y)}{\partial y^2}\,; \qquad \mathcal{V}(y,t) = EI\sum_{j=1}^{N_\mathrm{s}} Z_j(t)\frac{\partial^3\psi_j(y)}{\partial y^3} \tag{25}$$

in which the second and third derivatives of mode shapes ψ_j, $j = 1 \ldots N_\mathrm{s}$, are given in Appendix A, and where the time-domain generalized coordinates Z_j are given by the Fourier integrals

$$Z_j(t) = \frac{1}{2\pi}\int_{-\infty}^{\infty} \bar{Z}_j(\omega)\,\bar{\ddot{u}}_\mathrm{g}(\omega)\,\mathrm{e}^{\mathrm{i}\omega t}\,\mathrm{d}\omega\,; \qquad \ddot{Z}_j(t) = -\frac{1}{2\pi}\int_{-\infty}^{\infty} \omega^2\bar{Z}_j(\omega)\,\bar{\ddot{u}}_\mathrm{g}(\omega)\,\mathrm{e}^{\mathrm{i}\omega t}\,\mathrm{d}\omega \tag{26}$$

with $\bar{\ddot{u}}_\mathrm{g}(\omega)$ denoting the Fourier transform of the ground acceleration $\ddot{u}_\mathrm{g}(t)$, given by

$$\bar{\ddot{u}}_\mathrm{g}(\omega) = \int_0^{t_a} \ddot{u}_\mathrm{g}(t)\,\mathrm{e}^{-\mathrm{i}\omega t}\,\mathrm{d}t \tag{27}$$

2.4 Evaluation of the natural frequencies of coupled beam-fluid systems

The resonant frequencies of a vibrating beam-fluid system is an important feature characterizing its dynamic behavior. These frequencies can be approximated by the frequencies $\widetilde{\omega}_j$, $j=1\ldots N_\mathrm{s}$, that maximize or make infinite the generalized coordinates $\bar{Z}_j$. For this purpose, simplified frequency-dependent expressions of the generalized coordinates need to be obtained first. If only the first structural beam mode is included in the analysis, i.e. fundamental mode analysis, Eq. (3) simplifies to

$$\bar{S}_{1,1}(\omega)\,\bar{Z}_1(\omega) = \bar{Q}_1 \tag{28}$$

and the only generalized coordinate $\bar{Z}_1$ is then given by

$$\bar{Z}_1(\omega) = \frac{\bar{Q}_1}{\bar{S}_{1,1}(\omega)} \tag{29}$$

Therefore, the coupled vibration frequency $\widetilde{\omega}_1$ in a fundamental mode analysis can be obtained by solving the equation

$$S_{1,1}(\widetilde{\omega}_1) = 0 \tag{30}$$

which corresponds to an infinite generalized coordinate $\bar{Z}_1$. Using Eq. (20) with null damping yields

$$\widetilde{\omega}_1^2 = \frac{\pi\,\omega_1^2\,\mu_\mathrm{s}\,H\,M^*}{\pi\mu_\mathrm{s}\,H\,M^* + 4\rho_\mathrm{f}\,\Lambda_\mathrm{f}\,H^2\,\theta_{1,1}^*} \tag{31}$$

or according to Eq. (22)

$$\widetilde{\omega}_1 = \frac{\alpha\beta_1^2}{\sqrt{1+\zeta\,\theta_{1,1}^*}} \tag{32}$$

where the parameter ζ is defined by

$$\zeta = \frac{4\rho_\mathrm{f}\,\Lambda_\mathrm{f}\,H}{\pi\,\mu_\mathrm{s}\,M^*} \tag{33}$$

Eq. (32) can also be expressed in terms of the ratio Ω_1 of the fundamental frequencies of wet to dry beams

$$\Omega_1 = \frac{\widetilde{\omega}_1}{\omega_1} = \frac{1}{\sqrt{1+\zeta\,\theta_{1,1}^*}} \tag{34}$$

If two beam modes are included in the analysis, the system of equations (3) takes the form

$$\begin{bmatrix} \bar{S}_{1,1}(\omega) & \bar{S}_{1,2}(\omega) \\ \bar{S}_{1,2}(\omega) & \bar{S}_{2,2}(\omega) \end{bmatrix} \begin{bmatrix} \bar{Z}_1 \\ \bar{Z}_2 \end{bmatrix} = \begin{bmatrix} \bar{Q}_1 \\ \bar{Q}_2 \end{bmatrix} \tag{35}$$

yielding the generalized coordinates

$$\bar{Z}_1(\omega) = \frac{\bar{S}_{2,2}(\omega)\,\bar{Q}_1 - \bar{S}_{1,2}(\omega)\,\bar{Q}_2}{\det\begin{bmatrix}\bar{S}_{1,1}(\omega) & \bar{S}_{1,2}(\omega)\\ \bar{S}_{1,2}(\omega) & \bar{S}_{2,2}(\omega)\end{bmatrix}} = \frac{\bar{S}_{2,2}(\omega)\,\bar{Q}_1 - \bar{S}_{1,2}(\omega)\,\bar{Q}_2}{\bar{S}_{1,1}(\omega)\bar{S}_{2,2}(\omega) - \bar{S}^2_{1,2}(\omega)} \tag{36}$$

$$\bar{Z}_2(\omega) = \frac{\bar{S}_{1,1}(\omega)\,\bar{Q}_2 - \bar{S}_{1,2}(\omega)\,\bar{Q}_1}{\det\begin{bmatrix}\bar{S}_{1,1}(\omega) & \bar{S}_{1,2}(\omega)\\ \bar{S}_{1,2}(\omega) & \bar{S}_{2,2}(\omega)\end{bmatrix}} = \frac{\bar{S}_{1,1}(\omega)\,\bar{Q}_2 - \bar{S}_{1,2}(\omega)\,\bar{Q}_1}{\bar{S}_{1,1}(\omega)\bar{S}_{2,2}(\omega) - \bar{S}^2_{1,2}(\omega)} \tag{37}$$

Eqs. (36) and (37) imply that the first and second coupled vibration frequencies $\widetilde{\omega}_1$ and $\widetilde{\omega}_2$, respectively, can be obtained by solving the equation

$$\det\begin{bmatrix}\bar{S}_{1,1}(\omega) & \bar{S}_{1,2}(\omega)\\ \bar{S}_{1,2}(\omega) & \bar{S}_{2,2}(\omega)\end{bmatrix} = \bar{S}_{1,1}(\omega)\,\bar{S}_{2,2}(\omega) - \bar{S}^2_{1,2}(\omega) = 0 \tag{38}$$

which corresponds to infinite generalized coordinates $\bar{Z}_1$ and $\bar{Z}_2$. Substituting $\bar{S}_{1,1}$, $\bar{S}_{1,2}$ and $\bar{S}_{2,2}$ by their expressions from Eq. (20) and simplifying, Eq. (38) can be transformed into the quadratic equation

$$A\,\chi^2 + B\,\chi + C = 0 \tag{39}$$

where $\chi = \omega^2$ and

$$\begin{aligned} A &= 1 + \zeta\left(\theta^*_{1,1} + \theta^*_{2,2}\right) + \zeta^2\left[\theta^*_{1,1}\,\theta^*_{2,2} - \left(\theta^*_{1,2}\right)^2\right]\\ B &= \omega_1^2 + \omega_2^2 + \zeta\left(\omega_1^2\,\theta^*_{2,2} + \omega_2^2\,\theta^*_{1,1}\right)\\ &= \alpha^2\left[\left(\beta_1^4 + \beta_2^4\right) + \zeta\left(\beta_1^4\,\theta^*_{2,2} + \beta_2^4\,\theta^*_{1,1}\right)\right]\\ C &= \omega_1^2\,\omega_2^2 = \alpha^2\,\beta_1^4\,\beta_2^4 \end{aligned} \tag{40}$$

The first and second coupled vibration frequencies $\widetilde{\omega}_1$ and $\widetilde{\omega}_2$ correspond then to the smallest $\chi^{(\text{min})}$ and largest $\chi^{(\text{max})}$ real positive roots of the quadratic equation (39), yielding

$$\widetilde{\omega}_1 = \sqrt{\chi^{(\text{min})}} \;<\; \widetilde{\omega}_2 = \sqrt{\chi^{(\text{max})}} \tag{41}$$

Closed-form expressions for higher coupled vibration frequencies, i.e. $N_\text{s} > 2$, are more difficult to obtain and cumbersome when successfully determined. These frequencies can then be determined numerically by finding the roots of equation

$$\det \bar{\mathbf{S}} = 0 \tag{42}$$

with null damping. An efficient numerical solution can be obtained by rewriting Eq. (20) with null damping as

$$\frac{\pi\,\bar{S}_{j,m}(\omega)}{4\rho_\text{f}\,\Lambda_\text{f}\,\omega^2 H^2} = \frac{1}{\zeta}\left(\frac{\omega_j^2}{\omega^2} - 1\right)\delta_{j,m} - \theta^*_{j,m} \tag{43}$$

Eq. (42) is then equivalent to

$$\det(\mathbf{D} - \mathbf{\Theta}^*) = 0 \tag{44}$$

where $\mathbf{\Theta}^*$ is the $N_\mathrm{s} \times N_\mathrm{s}$ matrix with elements $\theta^*_{j,m}$, $j = 1 \ldots N_\mathrm{s}$ and $m = 1 \ldots N_\mathrm{s}$, and $\mathbf{D}$ is a diagonal matrix with elements $d_{j,j}$, $j = 1 \ldots N_\mathrm{s}$, given by

$$d_{j,j} = \frac{1}{\zeta}\left(\frac{\omega_j^2}{\omega^2} - 1\right) = \frac{1}{\zeta}\left(\frac{\alpha^2\beta_j^4}{\omega^2} - 1\right) \tag{45}$$

Eq. (44) can be solved numerically to obtain coupled vibration frequencies $\widetilde{\omega}_j$, $j = 1 \ldots N_\mathrm{s}$. It is easily seen that Eq. (44) is equivalent to Eqs. (34) when only first beam mode is considered in the analysis and to Eq. (39) when only two beam modes are included.

An important result brought by Eq. (44) is that the ratios $\Omega_j = \widetilde{\omega}_j/\omega_j$, $j = 1 \ldots N_\mathrm{s}$, depend only on: (i) the parameter ζ, which is function of the fluid and beam material properties ρ_f and μ_s, the height of the beam H, the number of fluid domains in contact with the beam Λ_f and the generalized mass M^*, and (ii) the parameters $\theta^*_{j,m}$, $j,\ m = 1 \ldots N_\mathrm{s}$, which, as given by Eqs. (13), and (15) to (18), depend on the boundary conditions of the studied beam.

3 Illustrative examples

3.1 Beam-fluid systems studied

In this section, we assess the effectiveness of the proposed formulation in determining the dynamic response of beam-fluid systems. For illustration purposes, we consider a beam-water system where the beam has a height of $10\,\mathrm{m}$ and a unit square cross-section of $1\,\mathrm{m}^2$. We assume that the beam can be subjected to the CF, CP, CS, CC or PP boundary conditions illustrated in Figs. 1 and 2. Two beam materials are considered: (i) Concrete with a mass density $\rho_\mathrm{s} = 2440\,\mathrm{kg/m}^3$ and a modulus of elasticity $E = 25\,\mathrm{GPa}$; and (ii) Steel with a mass density $\rho_\mathrm{s} = 7850\,\mathrm{kg/m}^3$ and a modulus of elasticity $E = 200\,\mathrm{GPa}$. A water mass density $\rho_\mathrm{f} = 1000\,\mathrm{kg/m}^3$ is used and the effects of one and two water domains, i.e. $\Lambda_\mathrm{f} = 1$ and 2, are investigated. The proposed simplified technique presented in Section 2 was programmed using MATLAB® [33] and then applied to investigate the dynamic response of the concrete and steel beam-water systems. For comparison purposes, finite element analyses of the beam-water systems are also conducted using the software ADINA [34], where the beam and water domain(s) are discterized into 2-nodes beam finite elements and 4-node potential-based (acoustic) finite elements, respectively. The procedure used to obtain the dynamic response of the beam-fluid system is known as the $\phi - U$ formulation since it is expressed in terms of displacements U and velocity potentials ϕ as state variables in the beam and fluid domains, respectively. Details of the $\phi - U$ formulation can be found elsewhere [26, 35, 36]. In these finite element analyses, fluid-structure interaction is accounted for through special elements at the beam-fluid interface. Beam vibrations cause fluid motions normal to beam-fluid inter-

face, and the fluid induced-pressure cause additional hydrodynamic loads to act on the beam. In the present case of two-dimensional analysis, the beam-fluid interface elements are 2-node line segments, which connect 2-node beam elements to adjacent 4-node potential-based fluid elements on the fluid domain boundary. The potential and structural degrees of freedom are related through a compatibility boundary condition. The performance of the potential-based formulation and the fluid-structure interface elements was assessed in a previous work [26]. Semi-infinite water domain is simulated by a finite water domain with a rigid boundary condition applied at a certain distance, large enough to eliminate reflection of waves at the far end of the fluid domain.

3.2 Earthquake time-history response of the beam-water systems

We first validate the ability of the proposed formulation to evaluate earthquake time-history responses for displacements, accelerations, shear forces and bending moments. For brevity, the results are shown only for the beam-water systems having a Clamped-Free (CF) configuration, subjected to the horizontal acceleration component of Imperial Valley earthquake (1940) at El Centro illustrated in Fig. 3. Ten structural modes are included in the dynamic analysis of the concrete and steel beam-water systems and a constant hysteretic damping ratio $\eta = 0.1$ is considered. The results obtained using the proposed simplified technique and the finite element method are illustrated in Figs. 4 to 7. In these figures, time-history responses for displacement u_{A} and acceleration $\ddot{u}_{\mathrm{A}}$ at the beams's free end, as well as shear force $\mathcal{V}_{\mathrm{C}}$, and overturning bending moment $\mathcal{M}_{\mathrm{C}}$ at the base are nondimensionalized by the values $u_{\mathrm{st}} = (\rho_{\mathrm{f}}\, \mathrm{g} H^5)/(30EI)$, peak ground acceleration $|\ddot{u}_{\mathrm{g}}|_{\mathrm{max}}$, $\mathcal{V}_{\mathrm{st}} = (\rho_{\mathrm{f}}\, \mathrm{g} H^2)/2$ and $\mathcal{M}_{\mathrm{st}} = (\rho_{\mathrm{f}}\, \mathrm{g} H^3)/6$, respectively. As can be seen from Figs. 4 and 5 illustrating the responses over the first 20 s of the earthquake, the results of the proposed method and the advanced finite element technique are in excellent agrement for both concrete and steel beam-fluid systems. We can see that the extreme values of a given response quantity are obtained at different time instants depending on the number of water domains. For a better assessment of the quality of the predictions, Figs. 6 and 7 provide close up views of the responses of the concrete and steel beam-fluid systems over a short time interval between 1 and 5 s, respectively. For comparison purposes, the time-history responses of the dry concrete and steel beams are also superposed to the previous results. These close up views confirm that the proposed method and the advanced finite element technique yield practically identical results for both concrete and steel beam-fluid systems. They also show that the earthquake response of the beams is clearly affected by the fluid-structure interaction and the number of water domains in contact with the beam. When comparing the seismic behavior of the dry and wet beams, we clearly observe the amplification of the amplitudes of all the response quantities studied, which emphasizes the need to include fluid-structure interaction effects for such applications. The results also confirm that fluid-structure interaction modifies the natural vibration frequencies of the beam-fluid systems, a phenomena that will investigated further in the next two sections.

It is also important to compare the finite element solution and proposed method in terms of execution CPU times. For illustration purposes, this information is compared next for the computation of time-history accelerations at point A of the concrete beam-water system having a CF configuration, and subjected to El Centro earthquake as described previously. The same time step of 0.005 s is used in both techniques and 10 beam modes are included in the response. The CPU times are obtained using one core of a 2.33 GHz Intel® Core™ 2 Duo Processor T7600, yielding 780 s and 1500 s for the finite element solution applied to the beam vibrating in contact with one and two water domains, respectively, and 26 s for the proposed method applied to the beam vibrating in contact with one or two water domains. It is important to note that the previous execution times of the finite element solution do not include the tasks of modeling, meshing and post-processing, which can significantly add to the computational burden associated with finite elements. Therefore, we can clearly conclude about the high effectiveness of the proposed method in assessing the dynamic response of beam-fluid systems. It is also worth mentioning that, from a practical engineering standpoint, the proposed formulation constitutes an interesting alternative solution considering the fluid-structure modeling complexities and related high expertise generally involved when using advanced finite element software.

3.3 Frequency domain response of the beam-water systems

In the previous section, the response of the beam-fluid systems was studied in the time domain under the effect of an earthquake having a given frequency content. In this section, the frequency domain response of the beam-fluid systems is investigated. For this purpose, frequency response curves of beam lateral accelerations are determined using Eq. (1). For each beam configuration shown in Fig. 2, frequency responses are determined over a range from 0 to $20\,\omega_1$, where ω_1 denotes the fundamental frequency of the corresponding dry beam. The results are shown in Fig. 8 for the CF beam configuration and Fig. 9 for the other beam configurations, respectively. Only frequency response curves of the concrete beam-fluid systems are shown for the sake of brevity. Figs. 8 and 9 also illustrate the results obtained using coupled finite elements as well as those corresponding to the dry beams. It is clearly seen that the proposed method is in excellent agreement with the finite element solutions for all beam configurations studied. The results demonstrate the shift of resonant frequencies towards lower frequencies due to fluid-structure interaction. The amplitude of frequency shift varies as a function of the mode considered, the constitutive material of the beam, its boundary conditions, as well as the number of interacting reservoirs. Finally, the effects of various boundary conditions on the dynamic response of the concrete beam-fluid systems can also be observed by comparing the frequency response curves in Figs. 8 and 9. It is important however to interpret these curves in terms of frequency ratios ω/ω_1, keeping in mind that the fundamental frequency ω_1 of the corresponding dry beam also contains the effects of boundary conditions.

3.4 Coupled frequencies of the beam-water systems

In this section, we assess the efficiency of the proposed method in predicting the 10 first natural frequencies of the concrete and steel beams described previously. The natural frequencies are determined for all the above-described beam configurations and the results are expressed in terms of the frequency ratios

$$\Omega_j^{(\mathrm{FE})} = \frac{\widetilde{\omega}_j^{(\mathrm{FE})}}{\omega_j}\,; \qquad\qquad \Omega_j^{(\mathrm{PM})} = \frac{\widetilde{\omega}_j^{(\mathrm{PM})}}{\omega_j} \tag{46}$$

in which $j = 1 \ldots 10$, ω_j is the natural frequency of the dry beam computed using Eq. (22), and $\widetilde{\omega}_j^{(\mathrm{FE})}$ and $\widetilde{\omega}_j^{(\mathrm{PM})}$ denote the natural frequencies of the beam-water systems determined using finite elements (FE) and the proposed method (PM) described in Section 2.4, respectively. Tables 8 and 9 contain the obtained frequency ratios for concrete and steel beam-water systems, respectively. We clearly see that the ratios predicted by the proposed method and finite elements are practically identical independently of the constitutive material of the beam, the mode number and beam boundary conditions. The computed frequency ratios also emphasize the importance of beam-water interaction effects on the natural frequencies and consequently the dynamic response of the system. For example, in the case of the Sliding-Clamped (SC) beam configuration with water on two sides, the ratio of the natural frequency of the dry beam on the wet beam reaches 0.40 and 0.62 for the concrete and steel beam-water systems, respectively. For a given mode, the frequency ratios depend on the constitutive material of the beam, its boundary conditions and the number of fluid domains in contact with the beam. When comparing frequency ratios obtained for the concrete and steel beam-water systems, we see that the effect of fluid-structure interaction decreases with larger beam stiffness. We also observe that the frequency ratios tend towards unity for higher modes, implying that hydrodynamic effects on the natural frequencies diminish as a function of increasing vibration modes.

4 Conclusions

A new formulation was proposed to study the modal dynamic and earthquake response of flexible beam-type structures vibrating in contact with one or two fluid domains. The methodology developed extends available analytical solutions for mode shapes and natural vibration frequencies of slender beams with various boundary conditions to include the effects of fluid-structure interaction. Simplified expressions are then developed to determine the frequency- and time-domain dynamic response of coupled beam-fluid systems and predict their natural vibration frequencies. Two beam-fluid systems were selected to illustrate the application of the proposed method and validate the results against advanced coupled fluid-structure finite element solutions. We showed that the proposed technique gives an excellent assessment of (i) the earthquake and frequency responses of coupled beam-fluid systems, and (ii) the natural vibration frequencies independently of the mode number and beam boundary conditions.

The numerical results confirmed the importance of accounting for fluid-structure interaction effects which may reduce by more than twice the fundamental vibration frequency of the dry beam and amplify its response quantities. From a practical standpoint, the proposed procedure offers an obvious advantage when compared to advanced finite elements including fluid-structure interaction capabilities. In the latter case indeed, the complexity of constructing the finite element model of the beam-fluid system is added to the need to satisfy convergence criteria related to the number of elements or nodes in the beam model as well as the truncation length of the fluid domain. The proposed method can be easily implemented in day-to-day practice, and can be used efficiently either to predict the modal dynamic properties and response of beam-fluid systems for design purposes, evaluate such properties and response for existing beam-fluid systems, or extract dynamic properties of a dry beam based on available modal data of a beam-fluid system. Finally, the methodology proposed can be extended to other types of structures for which mode shapes and natural vibration frequencies can be evaluated or approximated using closed-form expressions.

Acknowledgements

The authors would like to acknowledge the financial support of the Natural Sciences and Engineering Research Council of Canada (NSERC) and the Quebec Fund for Research on Nature and Technology (FQRNT).

Appendix A

This appendix reviews the mode shapes ψ_j, $j=1\ldots N_\mathrm{s}$, of a slender beam and its derivatives as a function of the various boundary conditions illustrated in Fig. 2 [28, 30]:

– For Clamped-Free (CF), Clamped-Pinned (CP), Clamped-Sliding (CS) and Clamped-Clamped (CC) boundary conditions

$$\psi_j(y) = \cosh\left(\frac{\beta_j\, y}{H}\right) - \cos\left(\frac{\beta_j\, y}{H}\right) - \sigma_j\left[\sinh\left(\frac{\beta_j\, y}{H}\right) - \sin\left(\frac{\beta_j\, y}{H}\right)\right] \tag{A1}$$

$$\frac{\partial^2\psi_j(y)}{\partial y^2} = \frac{\beta_j^2}{H^2}\left\{\cosh\left(\frac{\beta_j\, y}{H}\right) + \cos\left(\frac{\beta_j\, y}{H}\right) - \sigma_j\left[\sinh\left(\frac{\beta_j\, y}{H}\right) + \sin\left(\frac{\beta_j\, y}{H}\right)\right]\right\} \tag{A2}$$

$$\frac{\partial^3\psi_j(y)}{\partial y^3} = \frac{\beta_j^3}{H^3}\left\{\sinh\left(\frac{\beta_j\, y}{H}\right) - \sin\left(\frac{\beta_j\, y}{H}\right) - \sigma_j\left[\cosh\left(\frac{\beta_j\, y}{H}\right) + \cos\left(\frac{\beta_j\, y}{H}\right)\right]\right\} \tag{A3}$$

where the parameters β_j and σ_j are given in Table A1 for the different boundary conditions.

– For Pinned-Pinned (PP) boundary conditions

$$\psi_j(y) = \sin\left(\frac{\beta_j\, y}{H}\right) \tag{A4}$$

$$\frac{\partial^2\psi_j(y)}{\partial y^2} = -\frac{\beta_j^2}{H^2}\sin\left(\frac{\beta_j\, y}{H}\right) \tag{A5}$$

$$\frac{\partial^3\psi_j(y)}{\partial y^3} = -\frac{\beta_j^3}{H^3}\cos\left(\frac{\beta_j\, y}{H}\right) \tag{A6}$$

where the parameters β_j are given in Table A1.

– For Pinned-Clamped (PC) and Sliding-Clamped (SC) boundary conditions, the mode shapes and their derivatives can be obtained by replacing the coordinate y by $(H-y)$ in the right hand sides of Eqs. (A4) to (A6).

The corresponding functions $\bar{\psi}_j$, $j=1\ldots N_\mathrm{s}$, in Eqs. (6), (7) and (15) are given by

– For Clamped-Free (CF), Clamped-Pinned (CP), Clamped-Sliding (CS) and Clamped-Clamped (CC) boundary conditions

$$\bar{\psi}_j(\bar{y}) = \cosh\left(\beta_j\,\bar{y}\right) - \cos\left(\beta_j\,\bar{y}\right) - \sigma_j\left[\sinh\left(\beta_j\,\bar{y}\right) - \sin\left(\beta_j\,\bar{y}\right)\right] \tag{A7}$$

– For Pinned-Pinned (PP) boundary conditions

$$\bar{\psi}_j(\bar{y}) = \sin\left(\beta_j\,\bar{y}\right) \tag{A8}$$

– For Pinned-Clamped (PC) and Sliding-Clamped (SC) boundary conditions

$$\begin{aligned}\bar{\psi}_j(\bar{y}) = &\cosh\left[\beta_j\,(1-\bar{y})\right] - \cos\left[\beta_j\,(1-\bar{y})\right] \\ &- \sigma_j\Big\{\sinh\left[\beta_j\,(1-\bar{y})\right] - \sin\left[\beta_j\,(1-\bar{y})\right]\Big\}\end{aligned} \tag{A9}$$

References

[1] H.M. Westergaard, Water pressures on dams during earthquakes. Transactions, ASCE 98 (1933) 418–472.

[2] L.S. Jacobsen, Impulsive hydrodynamics of fluid inside a cylindrical tank and of fluid surrounding a cylindrical pier. Bulletin of the Seismological Society of America 39 (1949) 189–1949.

[3] P.V. Rao, Calculation of added mass of circular and rectangular piers oscillating in water. Proceedingd of the Fifth Symposium of Earthquake Engineering (1974) 97.

[4] H. Goto, K. Toki, Vibrational characteristics and aseismic design of submerged bridge piers. Proceedings of the Third World Conference on Earthguake Engineering, Vol. II, New Zealand, 1965 pp. 107–122.

[5] S. Kotsubo, Seismic force effect on submerged bridge piers with elliptic cross-sections. Proceedings of the Third World Conference on Earthguake Engineering, Vol. II, New Zealand, 1965 pp. 342–356.

[6] A. K. Chopra, Earthquake behavior of reservoir-dam systems. Journal of the Engineering Mechanics Division, ASCE, 94, No. EM6, (1968) 1475–1500.

[7] A. K. Chopra, Earthquake response of concrete gravity dams. Journal of the Engineering Mechanics Division, ASCE, 96, No. EM4, (1970) 443–454.

[8] O.C. Zienkiewicz, R.E. Newton, Coupled vibration of a structure submerged in a compressible fluid. Proceedings of the International Symposium of Finite Element Techniques, Vol. 15, 1969, pp. 1-–15.

[9] A.R. Chardrasekaran, S.S. Saini, M.M. Malhotra, Hydrodynamic pressure on circular cylindrical cantilever structures surrounded by water. Fourth Symposium on Earthquake Engineering, Roorkee, India, 1970, pp. 161–171.

[10] C.Y. Liaw, A.K. Chopra, Dynamics of towers surrounded by water. International Journal Earthquake Engineering and Structural Dynamics 3 (1974), no. 1, 33—49.

[11] Y. Tanaka, R. T. Hudspeth, Restoring forces on vertical circular cylinders forced by earthquakes. International Journal Earthquake Engineering and Structural Dynamics 16 (1988), no. 1, 99—119.

[12] Han, R.P.S., Xu, H, Simple and accurate added mass model for hydrodynamic fluid-structure interaction analysis. Journal of the Franklin Institute 333B (1996), no. 6, 929–945.

[13] K. Nagaya, Transient response in flexure to general uni-directional loads of variable cross-section beam with concentrated tip inertias immersed in a fluid. Journal of Sound and Vibration 99 (1985), no. 3, 361-–378.

[14] A. Uscilowska, J.A. Kolodziej, Free vibration of immersed column carrying a tip mass. Journal of Sound and Vibration 216 (1998), 147-–157.

[15] H.R. Oz, Natural frequenciesof an immersed beam carrying a tip mass with rotatory inertia. Journal of Sound and Vibration 266 (2003) 1099-–1108.

[16] J.S. Wu, S.-H. Hsu, A unified approach for the free vibration analysis of an elastically supported immersed uniform beam carrying an eccentric tip mass with rotary inertia. Journal of Sound and Vibration 291 (2006), 1122–1147.

[17] J.S. Wu, K.-W. Chen, An alternative approach to the structural motion analysis of wedge-beam offshore structures supporting a load. Ocean Engineering 30 (2003), 1791–1806.

[18] Chang, J.Y., Liu, W.H, Some studies on the natural frequencies of immersed restrained column. Journal of Sound and Vibration, 130 (1989), no. 3, 516–524.

[19] Nagaya, K., Hai, Y., Seismic response of underwater members of variable cross section. Journal of Sound Vibration 103 (1985), 119–138.

[20] Xing, J.T., Price, W.G., Pomfret, M. J., Yam, L.H, Natural vibration of a beam-water interaction system. Journal of Sound and Vibration, 199 (1997), 491–512.

[21] S. Zhao, J.T. Xing, W.G. Price, Natural vibration of a flexible beam–water coupled system with a concentrated mass attached at the free end of the beam. Proceedings of the Institution of Mechanical Engineers, Part M: Journal of Engineering for the Maritime Environment, Vol. 216, no. 2, 2002, pp. 145–154.

[22] J.T. Xing, Natural vibration of two-dimensional slender structure–water interaction systems subject to Sommerfeld radiation condition. Journal of Sound and Vibration 308 (2007) 67-–79.

[23] J. Nasserzare, Y. Lei, S. Eskandari-Shiri, Computation of natural frequencies and mode shapes of arch dams as an inverse problem. Advances in Engineering Software 31 (2000), no.11, 827–836

[24] S.M. de Souza, L.J. Pedroso, Study of flexible wall acoustic cavities using Beam Finite Element. Mechanics of Solids in Brazil, Brazilian Society of Mechanical Sciences and Engineering, H.S. da Costa Mattos & Marcílio Alves (Editors), 2009, pp. 223–237.

[25] G. Fenves, A.K. Chopra, Earthquake analysis and response of concrete gravity dams. Report No. UCB/EERC-84/10, University of California, Berkeley, California, 1984.

[26] N. Bouaanani, F.Y. Lu, Assessment of potential-based fluid finite elements for seismic analysis of dam–reservoir systems Journal of Computers and Structures 87 (2009) 206–224.

[27] B. Miquel, N. Bouaanani, Simplified evaluation of the vibration period and seismic response of gravity dam-water systems Journal of Engineering Structures 32 (2010) 2488–2502.

[28] D. Young, R. P., Jr. Felgar, Tables of characteristic functions representing normal modes of vibration of a beam. Engineering Research Series No. 44, Bureau of Engineering Research, Austin, Texas, 1949.

[29] T. Chang, R. R. Craig, Normal modes of uniform beams. Journal of Enginering Mechanics Division EM4(95) (1969), 1027—1031.

[30] Blevins RD. Formulas for natural frequency and mode shape. , Kriger publishing Company, Florida (1984) 296–297.

[31] Y. Tang, Numerical Evaluation of Uniform Beam Modes. Journal of Engineering Mechanics 129 (2003), 1475–1477.

[32] Higham, N. J, Accuracy and stability of numerical algorithms (Second ed.) SIAM, 2002.

[33] MATLAB ®. The Mathworks, Inc., Natick, MA, USA, 2011.

[34] ADINA Theory and Modeling Guide. Report ARD 10-7. ADINA R & D, Inc., 2010.

[35] Everstine GC. A symmetric potential formulation for fluid-structure interaction. Journal of Sound and Vibration 79 (1981) 157–160.

[36] Olson LG, Bathe KJ. Analysis of fluid-structure interactions: a direct symmetric coupled formulation based on the fluid velocity potential. Computers and Structures 21 (1985) 21–32.

List of tables

Table A1
Equations to determine parameters σ_j and β_j for modes $j = 1 \ldots N_s$.

Boundary conditions	σ_j	β_j is solution for:
Clamped-Free (CF)	$\frac{\sinh(\beta_j) - \sin(\beta_j)}{\cosh(\beta_j) + \cos(\beta_j)}$	$\cos(\beta_j)\cosh(\beta_j) + 1 = 0$
Clamped-Pinned (CP)	$\frac{\cosh(\beta_j) - \cos(\beta_j)}{\sinh(\beta_j) - \sin(\beta_j)}$	$\tan(\beta_j) - \tanh(\beta_j) = 0$
Pinned-Clamped (PC)	$\frac{\cosh(\beta_j) - \cos(\beta_j)}{\sinh(\beta_j) - \sin(\beta_j)}$	$\tan(\beta_j) - \tanh(\beta_j) = 0$
Clamped-Sliding (CS)	$\frac{\sinh(\beta_j) - \sin(\beta_j)}{\cosh(\beta_j) + \cos(\beta_j)}$	$\tan(\beta_j) + \tanh(\beta_j) = 0$
Sliding-Clamped (SC)	$\frac{\sinh(\beta_j) - \sin(\beta_j)}{\cosh(\beta_j) + \cos(\beta_j)}$	$\tan(\beta_j) + \tanh(\beta_j) = 0$
Clamped-Clamped (CC)	$\frac{\cosh(\beta_j) - \cos(\beta_j)}{\sinh(\beta_j) - \sin(\beta_j)}$	$\cos(\beta_j)\cosh(\beta_j) - 1 = 0$
Pinned-Pinned (PP)	–	$\beta_j = j\,\pi$

Table 1. Modal parameters for Clamped-Free beam configuration and modes $j = 1 \ldots 10$.

Mode	$j=1$	$j=2$	$j=3$	$j=4$	$j=5$	$j=6$	$j=7$	$j=8$	$j=9$	$j=10$
β_j	1.87510407	4.69409113	7.85475744	10.99554073	14.13716839	17.27875953	20.42035225	23.56194490	26.70353756	29.84513021
σ_j	0.73409551	1.01846732	0.99922450	1.00003355	0.99999855	1.00000006	1.00000000	1.00000000	1.00000000	1.00000000
M_j^*	1.00000000	1.00000000	1.00000000	1.00000000	1.00000000	1.00000000	1.00000000	1.00000000	1.00000000	1.00000000
L_j^*	0.78299176	0.43393590	0.25442530	0.18189802	0.14147084	0.11574906	0.09794150	0.08488264	0.07489644	0.06701261
Γ_j^*	-0.37664436	-0.45319221	-0.21267495	-0.17682201	-0.12338252	-0.11015766	-0.08674703	-0.07997306	-0.06687042	-0.06276876
$\theta_{1,j}^*$	0.18737428	0.13891965	0.02306732	0.04698614	0.01900129	0.02711927	0.01480436	0.01889087	0.01199198	0.01445421
$\theta_{2,j}^*$	0.13891965	0.25471077	0.10086194	0.04923220	0.05446351	0.03399742	0.03656928	0.02589163	0.02740289	0.02088616
$\theta_{3,j}^*$	0.02306732	0.10086194	0.14743433	0.05443936	0.03073993	0.03478738	0.02265145	0.02509607	0.01791674	0.01951888
$\theta_{4,j}^*$	0.04698614	0.04923220	0.05443936	0.10091067	0.03428665	0.02087210	0.02404472	0.01612420	0.01824417	0.01312597
$\theta_{5,j}^*$	0.01900129	0.05446351	0.03073993	0.03428665	0.07599235	0.02378298	0.01528846	0.01773461	0.01220999	0.01397671
$\theta_{6,j}^*$	0.02711927	0.03399742	0.03478738	0.02087210	0.02378298	0.06045095	0.01753848	0.01169707	0.01364568	0.00958498
$\theta_{7,j}^*$	0.01480436	0.03656928	0.02265145	0.02404472	0.01528846	0.01753848	0.05001153	0.01352421	0.00928712	0.01086720
$\theta_{8,j}^*$	0.01889087	0.02589163	0.02509607	0.01612420	0.01773461	0.01169707	0.01352421	0.04251876	0.01077686	0.00756417
$\theta_{9,j}^*$	0.01199198	0.02740289	0.01791674	0.01824417	0.01220999	0.01364568	0.00928712	0.01077686	0.03692034	0.00882309
$\theta_{10,j}^*$	0.01445421	0.02088616	0.01951888	0.01312597	0.01397671	0.00958498	0.01086720	0.00756417	0.00882309	0.03261731

Table 2. Modal parameters for Clamped-Pinned beam configuration and modes $j = 1 \ldots 10$.

Mode	$j=1$	$j=2$	$j=3$	$j=4$	$j=5$	$j=6$	$j=7$	$j=8$	$j=9$	$j=10$
β_j	3.92660231	7.06858275	10.21017612	13.35176878	16.49336143	19.63495408	22.77654674	25.91813939	29.05973205	32.20132470
σ_j	1.00077731	1.00000145	1.00000000	1.00000000	1.00000000	1.00000000	1.00000000	1.00000000	1.00000000	1.00000000
M_j^*	1.00000000	1.00000000	1.00000000	1.00000000	1.00000000	1.00000000	1.00000000	1.00000000	1.00000000	1.00000000
L_j^*	0.86000091	0.08263119	0.33438600	0.04387308	0.20700531	0.02983386	0.14990040	0.02260141	0.11748951	0.01819138
Γ_j^*	-0.57463863	-0.22387192	-0.19610132	-0.12740364	-0.11747947	-0.08877191	-0.08379277	-0.06808364	-0.06510595	-0.05520717
$\theta_{1,j}^*$	0.34894675	0.09636523	0.06874613	0.05303582	0.04307624	0.03623730	0.03126201	0.02748370	0.02451824	0.02212942
$\theta_{2,j}^*$	0.09636523	0.18069842	0.05207102	0.04099493	0.03360924	0.02840662	0.02456921	0.02163183	0.01931528	0.01744349
$\theta_{3,j}^*$	0.06874613	0.05207102	0.11733903	0.03252944	0.02700876	0.02299635	0.01997772	0.01763762	0.01577671	0.01426464
$\theta_{4,j}^*$	0.05303582	0.04099493	0.03252944	0.08546839	0.02239573	0.01922570	0.01679337	0.01488069	0.01334402	0.01208618
$\theta_{5,j}^*$	0.04307624	0.03360924	0.02700876	0.02239573	0.06663395	0.01644885	0.01444871	0.01285527	0.01156183	0.01049458
$\theta_{6,j}^*$	0.03623730	0.02840662	0.02299635	0.01922570	0.01644885	0.05432145	0.01264531	0.01129619	0.01019113	0.00927239
$\theta_{7,j}^*$	0.03126201	0.02456921	0.01997772	0.01679337	0.01444871	0.01264531	0.04569814	0.01005606	0.00909966	0.00829931
$\theta_{8,j}^*$	0.02748370	0.02163183	0.01763762	0.01488069	0.01285527	0.01129619	0.01005606	0.03934902	0.00820841	0.00750383
$\theta_{9,j}^*$	0.02451824	0.01931528	0.01577671	0.01334402	0.01156183	0.01019113	0.00909966	0.00820841	0.03449382	0.00684054
$\theta_{10,j}^*$	0.02212942	0.01744349	0.01426464	0.01208618	0.01049458	0.00927239	0.00829931	0.00750383	0.00684054	0.03066917

Table 3. Modal parameters for Pinned-Clamped beam configuration and modes $j = 1 \ldots 10$.

Mode	$j=1$	$j=2$	$j=3$	$j=4$	$j=5$	$j=6$	$j=7$	$j=8$	$j=9$	$j=10$
β_j	3.92660231	7.06858275	10.21017612	13.35176878	16.49336143	19.63495408	22.77654674	25.91813939	29.05973205	32.20132470
σ_j	1.00077731	1.00000145	1.00000000	1.00000000	1.00000000	1.00000000	1.00000000	1.00000000	1.00000000	1.00000000
M_j^*	1.00000000	1.00000000	1.00000000	1.00000000	1.00000000	1.00000000	1.00000000	1.00000000	1.00000000	1.00000000
L_j^*	0.86000091	0.08263119	0.33438600	0.04387308	0.20700531	0.02983386	0.14990040	0.02260141	0.11748951	0.01819138
Γ_j^*	-0.65008940	0.07630378	-0.18764735	0.06077168	-0.10437260	0.04753510	-0.07134179	0.03871620	-0.05389119	0.03288874
$\theta_{1,j}^*$	0.42517390	-0.05350698	0.08215456	-0.03863831	0.04827983	-0.02921415	0.03392985	-0.02331070	0.02608839	-0.01953294
$\theta_{2,j}^*$	-0.05350698	0.16093621	-0.02220990	0.02887463	-0.01573978	0.01957338	-0.01235525	0.01466114	-0.01016711	0.01167131
$\theta_{3,j}^*$	0.08215456	-0.02220990	0.11404365	-0.01510174	0.02319127	-0.01179012	0.01654423	-0.00971221	0.01275610	-0.00829536
$\theta_{4,j}^*$	-0.03863831	0.02887463	-0.01510174	0.07776274	-0.01002847	0.01349708	-0.00781427	0.01030195	-0.00648317	0.00825628
$\theta_{5,j}^*$	0.04827983	-0.01573978	0.02319127	-0.01002847	0.06298601	-0.00757148	0.01130633	-0.00620408	0.00884611	-0.00531480
$\theta_{6,j}^*$	-0.02921415	0.01957338	-0.01179012	0.01349708	-0.00757148	0.05001431	-0.00575588	0.00782770	-0.00473329	0.00637173
$\theta_{7,j}^*$	0.03392985	-0.01235525	0.01654423	-0.00781427	0.01130633	-0.00575588	0.04301687	-0.00464035	0.00679016	-0.00394881
$\theta_{8,j}^*$	-0.02331070	0.01466114	-0.00971221	0.01030195	-0.00620408	0.00782770	-0.00464035	0.03654155	-0.00376882	0.00515097
$\theta_{9,j}^*$	0.02608839	-0.01016711	0.01275610	-0.00648317	0.00884611	-0.00473329	0.00679016	-0.00376882	0.03250581	-0.00317360
$\theta_{10,j}^*$	-0.01953294	0.01167131	-0.00829536	0.00825628	-0.00531480	0.00637173	-0.00394881	0.00515097	-0.00317360	0.02868411

Table 4. Modal parameters for Clamped-Sliding beam configuration and modes $j = 1 \ldots 10$.

Mode	$j=1$	$j=2$	$j=3$	$j=4$	$j=5$	$j=6$	$j=7$	$j=8$	$j=9$	$j=10$
β_j	2.36502037	5.49780392	8.63937983	11.78097245	14.92256510	18.06415776	21.20575041	24.34734307	27.48893572	30.63052837
σ_j	0.98250221	0.99996645	0.99999994	1.00000000	1.00000000	1.00000000	1.00000000	1.00000000	1.00000000	1.00000000
M_j^*	1.00000000	1.00000000	1.00000000	1.00000000	1.00000000	1.00000000	1.00000000	1.00000000	1.00000000	1.00000000
L_j^*	0.83086152	0.36376941	0.23149808	0.16976527	0.13402522	0.11071648	0.09431404	0.08214449	0.07275655	0.06529434
Γ_j^*	-0.43286638	-0.42564791	-0.16756712	-0.18178678	-0.10517939	-0.11405106	-0.07681829	-0.08275793	-0.06056673	-0.06482797
$\theta_{1,j}^*$	0.22689238	0.14212397	0.02072279	0.05815096	0.01755383	0.03503476	0.01429268	0.02471378	0.01195579	0.01896470
$\theta_{2,j}^*$	0.14212397	0.25076545	0.08206426	0.05438069	0.04980423	0.03590995	0.03522013	0.02682757	0.02711837	0.02144159
$\theta_{3,j}^*$	0.02072279	0.08206426	0.12952878	0.04471812	0.02614002	0.02964005	0.01930793	0.02189888	0.01525828	0.01727970
$\theta_{4,j}^*$	0.05815096	0.05438069	0.04471812	0.09818121	0.02975176	0.02178165	0.02172608	0.01650675	0.01694890	0.01325951
$\theta_{5,j}^*$	0.01755383	0.04980423	0.02614002	0.02975176	0.07140048	0.02081032	0.01423315	0.01578391	0.01135808	0.01262290
$\theta_{6,j}^*$	0.03503476	0.03590995	0.02964005	0.02178165	0.02081032	0.05910759	0.01569605	0.01208765	0.01246242	0.00980901
$\theta_{7,j}^*$	0.01429268	0.03522013	0.01930793	0.02172608	0.01423315	0.01569605	0.04808431	0.01217323	0.00894149	0.00987213
$\theta_{8,j}^*$	0.02471378	0.02682757	0.02189888	0.01650675	0.01578391	0.01208765	0.01217323	0.04176229	0.00981895	0.00779709
$\theta_{9,j}^*$	0.01195579	0.02711837	0.01525828	0.01694890	0.01135808	0.01246242	0.00894149	0.00981895	0.03589457	0.00805705
$\theta_{10,j}^*$	0.01896470	0.02144159	0.01727970	0.01325951	0.01262290	0.00980901	0.00987213	0.00779709	0.00805705	0.03209606

Table 5. Modal parameters for Sliding-Clamped beam configuration and modes $j = 1 \ldots 10$.

Mode	$j=1$	$j=2$	$j=3$	$j=4$	$j=5$	$j=6$	$j=7$	$j=8$	$j=9$	$j=10$
β_j	2.36502037	5.49780392	8.63937983	11.78097245	14.92256510	18.06415776	21.20575041	24.34734307	27.48893572	30.63052837
σ_j	0.98250221	0.99996645	0.99999994	1.00000000	1.00000000	1.00000000	1.00000000	1.00000000	1.00000000	1.00000000
M_j^*	1.00000000	1.00000000	1.00000000	1.00000000	1.00000000	1.00000000	1.00000000	1.00000000	1.00000000	1.00000000
L_j^*	0.83086152	0.36376941	0.23149808	0.16976527	0.13402522	0.11071648	0.09431404	0.08214449	0.07275655	0.06529434
Γ_j^*	-0.68350770	-0.17189508	-0.07913826	-0.04607007	-0.03038167	-0.02165278	-0.01627248	-0.01271008	-0.01022374	-0.00842479
$\theta_{1,j}^*$	0.49079872	0.04802871	0.02127759	0.01179377	0.00745121	0.00512170	0.00373253	0.00283919	0.00223181	0.00180488
$\theta_{2,j}^*$	0.04802871	0.16975665	0.01534789	0.00949173	0.00633431	0.00448987	0.00333420	0.00256760	0.00203526	0.00165744
$\theta_{3,j}^*$	0.02127759	0.01534789	0.10157987	0.00743933	0.00533273	0.00395149	0.00302040	0.00237210	0.00190658	0.00155919
$\theta_{4,j}^*$	0.01179377	0.00949173	0.00743933	0.07236825	0.00437216	0.00339546	0.00268245	0.00215711	0.00176407	0.00146769
$\theta_{5,j}^*$	0.00745121	0.00633431	0.00533273	0.00437216	0.05617515	0.00287253	0.00234443	0.00193246	0.00161049	0.00135661
$\theta_{6,j}^*$	0.00512170	0.00448987	0.00395149	0.00339546	0.00287253	0.04589287	0.00202983	0.00171330	0.00145510	0.00124530
$\theta_{7,j}^*$	0.00373253	0.00333420	0.00302040	0.00268245	0.00234443	0.00202983	0.03878766	0.00150988	0.00130561	0.00113294
$\theta_{8,j}^*$	0.00283919	0.00256760	0.00237210	0.00215711	0.00193246	0.00171330	0.00150988	0.03358532	0.00116677	0.00102810
$\theta_{9,j}^*$	0.00223181	0.00203526	0.00190658	0.00176407	0.00161049	0.00145510	0.00130561	0.00116677	0.02961224	0.00092819
$\theta_{10,j}^*$	0.00180488	0.00165744	0.00155919	0.00146769	0.00135661	0.00124530	0.00113294	0.00102810	0.00092819	0.02648024

Table 6. Modal parameters for Clamped-Clamped beam configuration and modes $j = 1 \ldots 10$.

Mode	$j=1$	$j=2$	$j=3$	$j=4$	$j=5$	$j=6$	$j=7$	$j=8$	$j=9$	$j=10$
β_j	4.73004074	7.85320462	10.99560784	14.13716549	17.27875966	20.42035225	23.56194490	26.70353756	29.84513021	32.98672286
σ_j	0.98250221	1.00077731	0.99996645	1.00000145	0.99999994	1.00000000	1.00000000	1.00000000	1.00000000	1.00000000
M_j^*	1.00000000	1.00000000	1.00000000	1.00000000	1.00000000	1.00000000	1.00000000	1.00000000	1.00000000	1.00000000
L_j^*	0.83086152	0.00000000	0.36376941	0.00000000	0.23149808	0.00000000	0.16976527	0.00000000	0.13402522	0.00000000
Γ_j^*	-0.59868962	-0.13987318	-0.21855053	-0.09614570	-0.12945024	-0.07230322	-0.09122754	-0.05783276	-0.07018707	-0.04817068
$\theta_{1,j}^*$	0.37372242	0.06778702	0.08798799	0.04552238	0.05315634	0.03375798	0.03774868	0.02674651	0.02919134	0.02212455
$\theta_{2,j}^*$	0.06778702	0.15976063	0.03574881	0.03706915	0.02434856	0.02570896	0.01848378	0.01946197	0.01489814	0.01560600
$\theta_{3,j}^*$	0.08798799	0.03574881	0.11879885	0.02488654	0.03088926	0.01879745	0.02242843	0.01505866	0.01745499	0.01252814
$\theta_{4,j}^*$	0.04552238	0.03706915	0.02488654	0.08161727	0.01729534	0.01907456	0.01329269	0.01474782	0.01079770	0.01194277
$\theta_{5,j}^*$	0.05315634	0.02434856	0.03088926	0.01729534	0.06695049	0.01322241	0.01616154	0.01067716	0.01279461	0.00889309
$\theta_{6,j}^*$	0.03375798	0.02570896	0.01879745	0.01907456	0.01322241	0.05304073	0.01024572	0.01156979	0.00836101	0.00950373
$\theta_{7,j}^*$	0.03774868	0.01848378	0.02242843	0.01329269	0.01616154	0.01024572	0.04583325	0.00832049	0.01008492	0.00692673
$\theta_{8,j}^*$	0.02674651	0.01946197	0.01505866	0.01474782	0.01067716	0.01156979	0.00832049	0.03878603	0.00677053	0.00782252
$\theta_{9,j}^*$	0.02919134	0.01489814	0.01745499	0.01079770	0.01279461	0.00836101	0.01008492	0.00677053	0.03435888	0.00561147
$\theta_{10,j}^*$	0.02212455	0.01560600	0.01252814	0.01194277	0.00889309	0.00950373	0.00692673	0.00782252	0.00561147	0.02965831

Table 7. Modal parameters for Pinned-Pinned beam configuration and modes $j = 1 \ldots 10$.

Mode	$j=1$	$j=2$	$j=3$	$j=4$	$j=5$	$j=6$	$j=7$	$j=8$	$j=9$	$j=10$
β_j	3.14159265	6.28318531	9.42477796	12.56637061	15.70796327	18.84955592	21.99114858	25.13274123	28.27433388	31.41592654
M_j^*	0.50000000	0.50000000	0.50000000	0.50000000	0.50000000	0.50000000	0.50000000	0.50000000	0.50000000	0.50000000
L_j^*	0.63661977	0.00000000	0.21220659	0.00000000	0.12732395	0.00000000	0.09094568	0.00000000	0.07073553	0.00000000
Γ_j^*	-0.45071585	-0.11925463	-0.11251300	-0.06569036	-0.06362745	-0.04530423	-0.04431800	-0.03456940	-0.03399328	-0.02794578
$\theta_{1,j}^*$	0.20264237	0.04503164	0.03152215	0.02418842	0.01959948	0.01646314	0.01418643	0.01245973	0.01110584	0.01001614
$\theta_{2,j}^*$	0.04503164	0.09006327	0.01981392	0.01543942	0.01263337	0.01068283	0.00924963	0.00815278	0.00728676	0.00658589
$\theta_{3,j}^*$	0.03152215	0.01981392	0.05613944	0.01139576	0.00939231	0.00798396	0.00694015	0.00613585	0.00549732	0.00497825
$\theta_{4,j}^*$	0.02418842	0.01543942	0.01139576	0.04028953	0.00749098	0.00639410	0.00557609	0.00494253	0.00443741	0.00402531
$\theta_{5,j}^*$	0.01959948	0.01263337	0.00939231	0.00749098	0.03123378	0.00533858	0.00466794	0.00414652	0.00372942	0.00338815
$\theta_{6,j}^*$	0.01646314	0.01068283	0.00798396	0.00639410	0.00533858	0.02541751	0.00401713	0.00357494	0.00322029	0.00292945
$\theta_{7,j}^*$	0.01418643	0.00924963	0.00694015	0.00557609	0.00466794	0.00401713	0.02138386	0.00314341	0.00283535	0.00258224
$\theta_{8,j}^*$	0.01245973	0.00815278	0.00613585	0.00494253	0.00414652	0.00357494	0.00314341	0.01843053	0.00253352	0.00230969
$\theta_{9,j}^*$	0.01110584	0.00728676	0.00549732	0.00443741	0.00372942	0.00322029	0.00283535	0.00253352	0.01617910	0.00208975
$\theta_{10,j}^*$	0.01001614	0.00658589	0.00497825	0.00402531	0.00338815	0.00292945	0.00258224	0.00230969	0.00208975	0.01440835

Table 8. Wet to dry frequency ratios for concrete beam-water system.

Configuration	Λ_f	Ratio	Vibration mode number									
			1	2	3	4	5	6	7	8	9	10
CF	1	$\eta^{(FE)}$	0.71	0.69	0.78	0.83	0.86	0.88	0.90	0.91	0.92	0.93
		$\eta^{(PM)}$	0.71	0.69	0.78	0.83	0.86	0.89	0.90	0.91	0.92	0.93
	2	$\eta^{(FE)}$	0.58	0.58	0.67	0.73	0.77	0.81	0.83	0.85	0.86	0.88
		$\eta^{(PM)}$	0.58	0.58	0.67	0.73	0.78	0.81	0.83	0.85	0.87	0.88
CP	1	$\eta^{(FE)}$	0.59	0.73	0.80	0.85	0.87	0.89	0.91	0.92	0.93	0.93
		$\eta^{(PM)}$	0.59	0.73	0.81	0.85	0.87	0.89	0.91	0.92	0.93	0.93
	2	$\eta^{(FE)}$	0.46	0.61	0.69	0.75	0.79	0.82	0.84	0.86	0.87	0.88
		$\eta^{(PM)}$	0.46	0.61	0.70	0.75	0.79	0.82	0.84	0.86	0.87	0.88
PC	1	$\eta^{(FE)}$	0.55	0.74	0.81	0.85	0.88	0.90	0.91	0.92	0.93	0.94
		$\eta^{(PM)}$	0.56	0.74	0.81	0.85	0.88	0.90	0.91	0.92	0.93	0.94
	2	$\eta^{(FE)}$	0.43	0.61	0.70	0.75	0.79	0.82	0.84	0.86	0.87	0.88
		$\eta^{(PM)}$	0.43	0.62	0.70	0.76	0.79	0.82	0.84	0.86	0.87	0.88
CS	1	$\eta^{(FE)}$	0.67	0.69	0.79	0.83	0.87	0.89	0.90	0.91	0.92	0.93
		$\eta^{(PM)}$	0.68	0.70	0.79	0.84	0.87	0.89	0.90	0.92	0.92	0.93
	2	$\eta^{(FE)}$	0.54	0.58	0.68	0.74	0.78	0.81	0.83	0.85	0.87	0.88
		$\eta^{(PM)}$	0.54	0.58	0.68	0.74	0.78	0.81	0.83	0.85	0.87	0.88
SC	1	$\eta^{(FE)}$	0.53	0.73	0.81	0.85	0.88	0.90	0.91	0.92	0.93	0.94
		$\eta^{(PM)}$	0.53	0.73	0.81	0.85	0.88	0.90	0.91	0.92	0.93	0.94
	2	$\eta^{(FE)}$	0.40	0.60	0.70	0.75	0.79	0.82	0.84	0.86	0.87	0.89
		$\eta^{(PM)}$	0.40	0.61	0.70	0.76	0.80	0.82	0.84	0.86	0.87	0.89
CC	1	$\eta^{(FE)}$	0.58	0.74	0.80	0.85	0.87	0.89	0.91	0.92	0.93	0.93
		$\eta^{(PM)}$	0.58	0.75	0.81	0.85	0.87	0.89	0.91	0.92	0.93	0.94
	2	$\eta^{(FE)}$	0.45	0.62	0.70	0.75	0.79	0.82	0.84	0.86	0.87	0.88
		$\eta^{(PM)}$	0.45	0.62	0.70	0.75	0.79	0.82	0.84	0.86	0.87	0.89
PP	1	$\eta^{(FE)}$	0.56	0.73	0.80	0.85	0.88	0.89	0.91	0.92	0.93	0.94
		$\eta^{(PM)}$	0.57	0.73	0.81	0.85	0.88	0.90	0.91	0.92	0.93	0.94
	2	$\eta^{(FE)}$	0.43	0.60	0.69	0.75	0.79	0.82	0.84	0.86	0.87	0.88
		$\eta^{(PM)}$	0.44	0.61	0.70	0.75	0.79	0.82	0.84	0.86	0.87	0.88

Table 9. Wet to dry frequency ratios for steel beam-water system.

Configuration	Λ_f	Ratio	Vibration mode number									
			1	2	3	4	5	6	7	8	9	10
CF	1	$\eta^{(FE)}$	0.88	0.85	0.91	0.93	0.95	0.96	0.96	0.97	0.97	0.98
		$\eta^{(PM)}$	0.88	0.85	0.91	0.93	0.95	0.96	0.96	0.97	0.97	0.98
	2	$\eta^{(FE)}$	0.79	0.77	0.84	0.88	0.91	0.92	0.93	0.94	0.95	0.96
		$\eta^{(PM)}$	0.79	0.77	0.84	0.88	0.91	0.92	0.93	0.94	0.95	0.95
CP	1	$\eta^{(FE)}$	0.80	0.88	0.92	0.94	0.95	0.96	0.97	0.97	0.98	0.98
		$\eta^{(PM)}$	0.80	0.88	0.92	0.94	0.95	0.96	0.97	0.97	0.97	0.98
	2	$\eta^{(FE)}$	0.68	0.81	0.86	0.89	0.91	0.93	0.94	0.95	0.95	0.96
		$\eta^{(PM)}$	0.68	0.81	0.86	0.89	0.91	0.93	0.94	0.95	0.95	0.96
PC	1	$\eta^{(FE)}$	0.77	0.89	0.92	0.94	0.96	0.96	0.97	0.97	0.98	0.98
		$\eta^{(PM)}$	0.77	0.89	0.92	0.94	0.95	0.96	0.97	0.97	0.98	0.98
	2	$\eta^{(FE)}$	0.65	0.81	0.86	0.90	0.92	0.93	0.94	0.95	0.95	0.96
		$\eta^{(PM)}$	0.65	0.81	0.86	0.90	0.92	0.93	0.94	0.95	0.95	0.96
CS	1	$\eta^{(FE)}$	0.86	0.85	0.91	0.93	0.95	0.96	0.97	0.97	0.97	0.98
		$\eta^{(PM)}$	0.85	0.85	0.91	0.93	0.95	0.96	0.97	0.97	0.97	0.98
	2	$\eta^{(FE)}$	0.76	0.77	0.85	0.88	0.91	0.92	0.94	0.94	0.95	0.96
		$\eta^{(PM)}$	0.76	0.77	0.85	0.88	0.91	0.92	0.94	0.94	0.95	0.96
SC	1	$\eta^{(FE)}$	0.75	0.89	0.93	0.95	0.96	0.97	0.97	0.97	0.98	0.98
		$\eta^{(PM)}$	0.75	0.89	0.93	0.95	0.96	0.96	0.97	0.97	0.98	0.98
	2	$\eta^{(FE)}$	0.62	0.81	0.87	0.90	0.92	0.93	0.94	0.95	0.96	0.96
		$\eta^{(PM)}$	0.62	0.81	0.87	0.90	0.92	0.93	0.94	0.95	0.96	0.96
CC	1	$\eta^{(FE)}$	0.79	0.89	0.92	0.94	0.95	0.96	0.97	0.97	0.98	0.98
		$\eta^{(PM)}$	0.79	0.89	0.92	0.94	0.95	0.96	0.97	0.97	0.97	0.98
	2	$\eta^{(FE)}$	0.67	0.82	0.86	0.90	0.92	0.93	0.94	0.95	0.95	0.96
		$\eta^{(PM)}$	0.67	0.82	0.86	0.90	0.91	0.93	0.94	0.95	0.95	0.96
PP	1	$\eta^{(FE)}$	0.78	0.88	0.92	0.94	0.96	0.96	0.97	0.97	0.98	0.98
		$\eta^{(PM)}$	0.78	0.88	0.92	0.94	0.95	0.96	0.97	0.97	0.98	0.98
	2	$\eta^{(FE)}$	0.66	0.80	0.86	0.90	0.92	0.93	0.94	0.95	0.95	0.96
		$\eta^{(PM)}$	0.66	0.80	0.86	0.90	0.92	0.93	0.94	0.95	0.95	0.96

List of figures

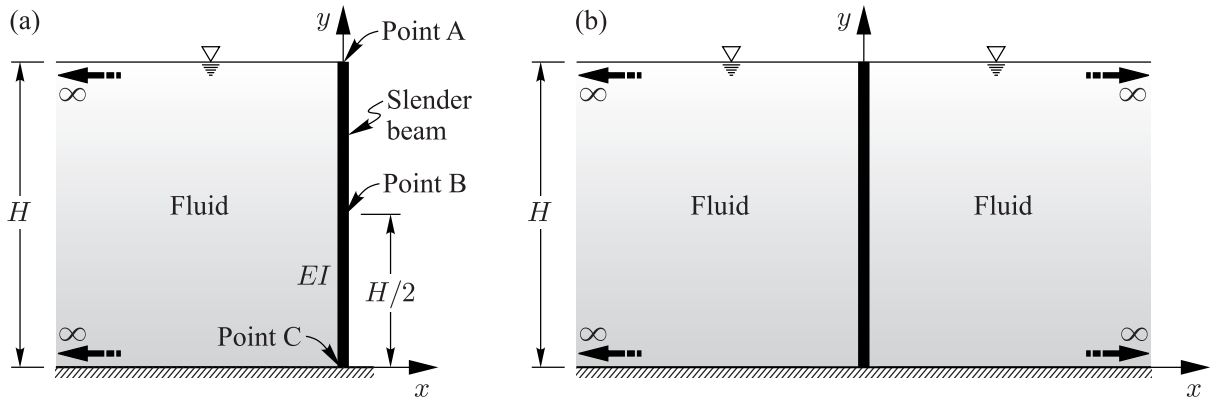

Figure 1. Slender beam vibrating in contact with a fluid acting on: (a) one side, (b) both sides.

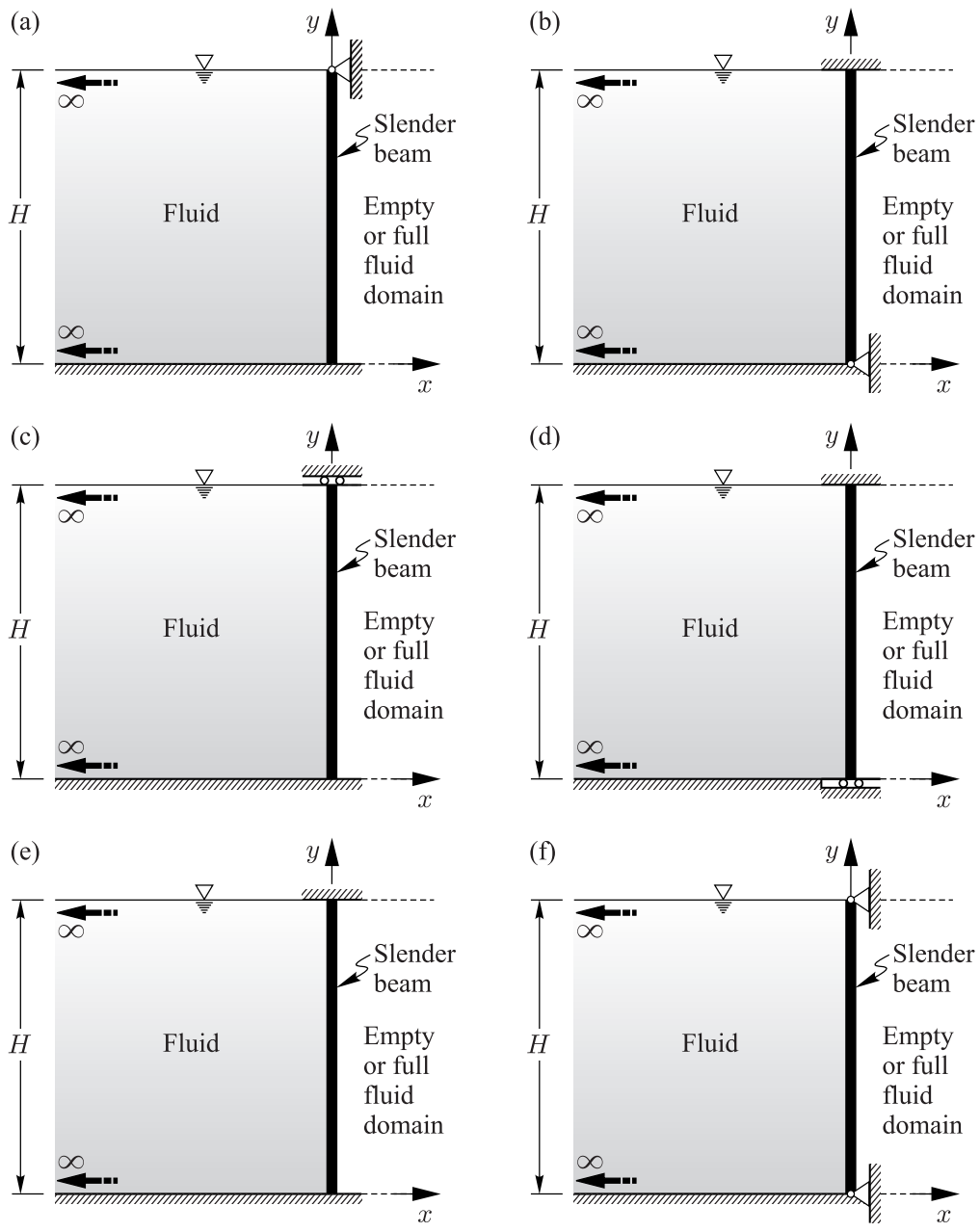

Figure 2. Studied beams-fluid configurations: (a) Clamped-Pinned (CP); (b) Pinned-Clamped (PC); (c) Clamped-Sliding (CS); (d) Sliding-Clamped (SC); (e) Clamped-Clamped (CC); (f) Pinned-Pinned (PP).

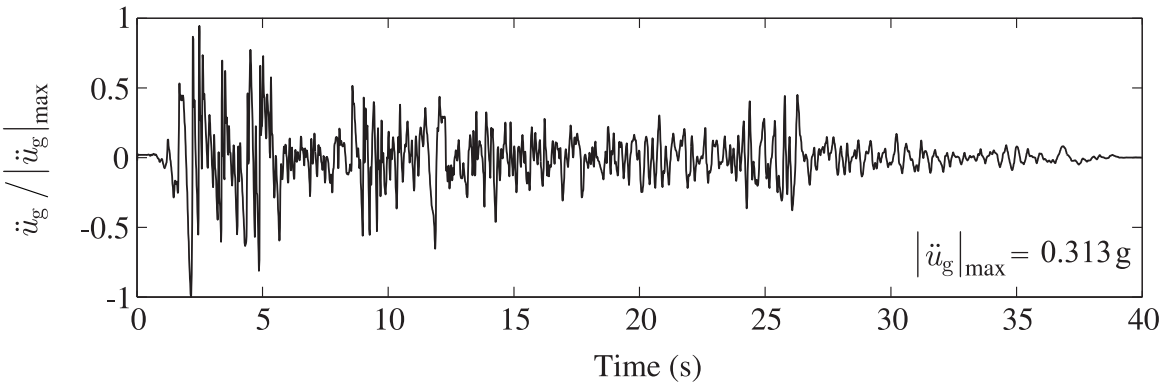

Figure 3. Horizontal acceleration component of Imperial Valley earthquake (1940) at El Centro.

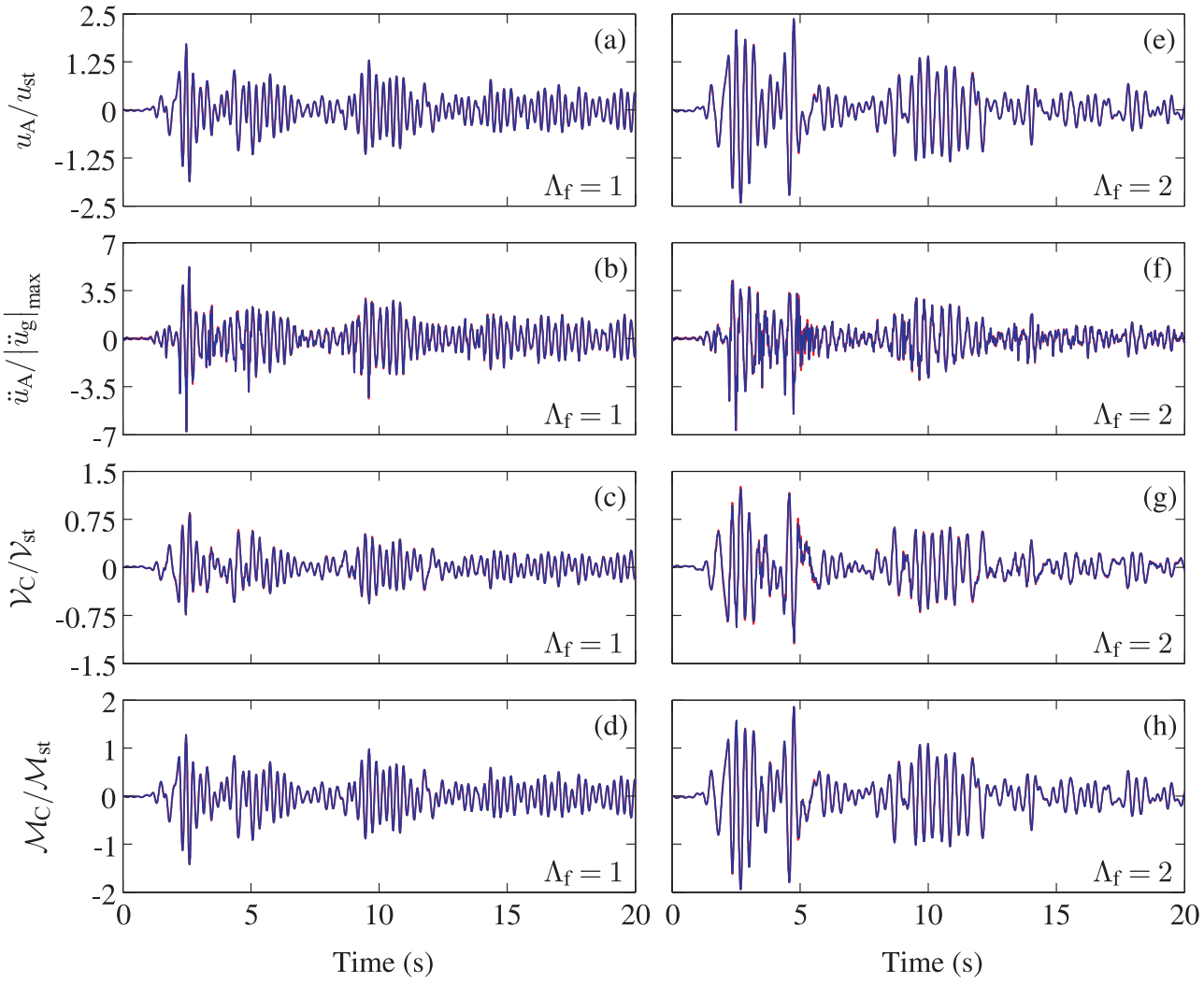

Figure 4. Time-history responses of the concrete beam-fluid system - CF configuration: (a) and (e) Displacement at the top; (b) and (f) Acceleration at the top; (c) and (g) Shear force at the base; (d) and (h) Bending moment at the base. (a) to (d) Beam in contact with water on one side; (e) to (h) beam in contact with water on two sides. — Finite elements (Wet beam); — Proposed method (Wet beam).

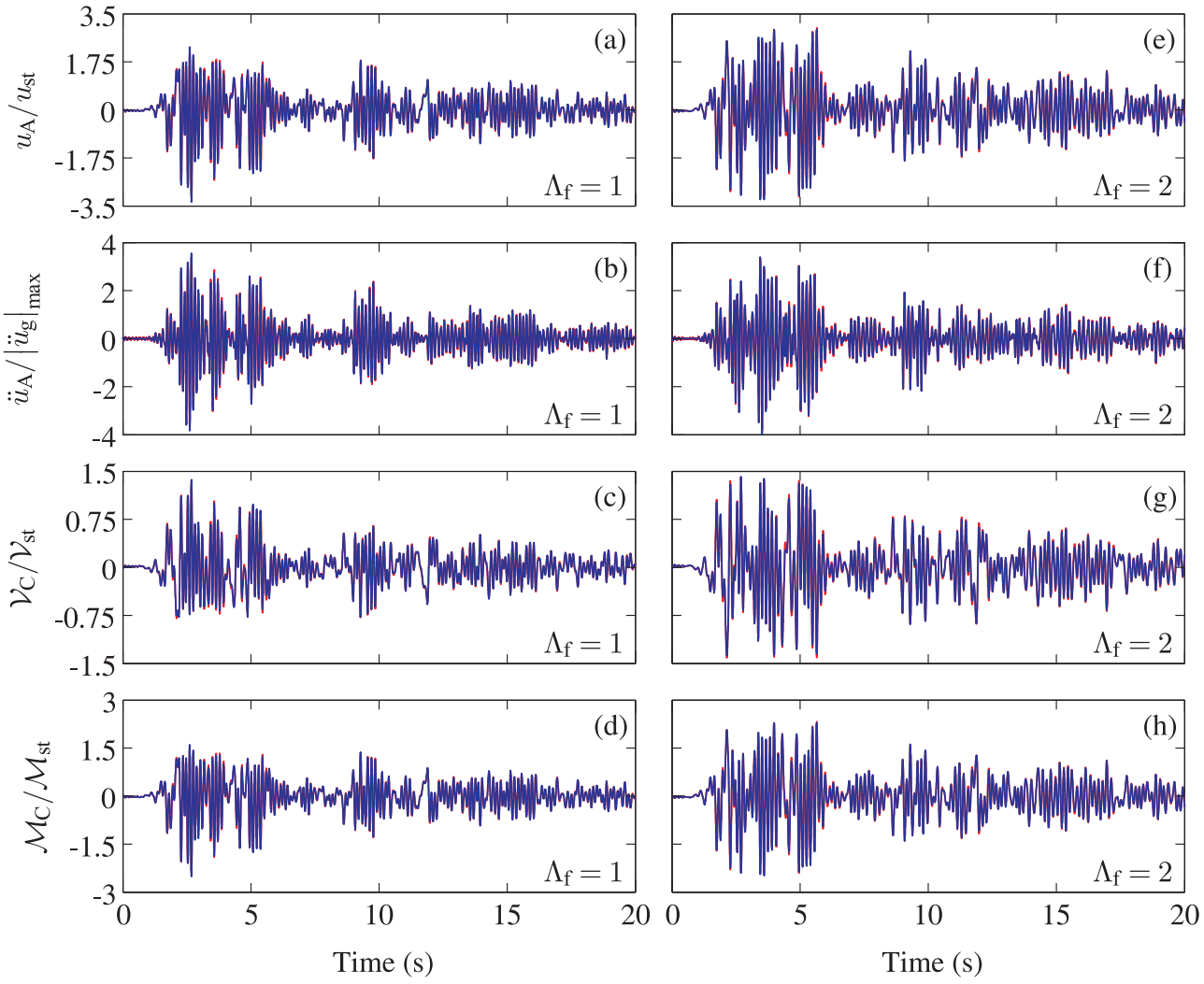

Figure 5. Time-history responses of the steel beam-fluid system - CF configuration: (a) and (e) Displacement at the top; (b) and (f) Acceleration at the top; (c) and (g) Shear force at the base; (d) and (h) Bending moment at the base. (a) to (d) Beam in contact with water on one side; (e) to (h) beam in contact with water on two sides. — Finite elements (Wet beam); — Proposed method (Wet beam).

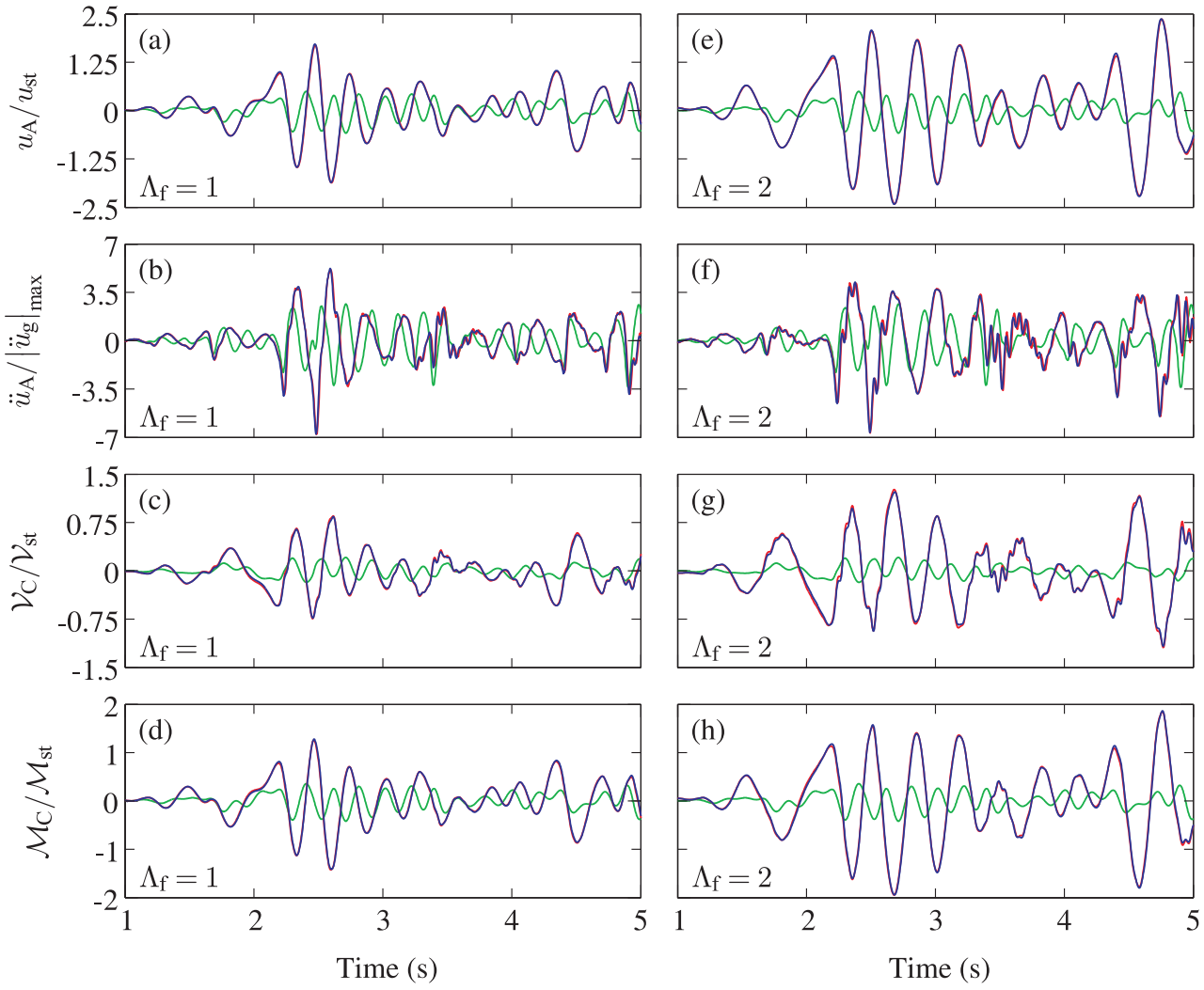

Figure 6. Time-history responses of the concrete beam-fluid system - CF configuration: (a) and (e) Displacement at the top; (b) and (f) Acceleration at the top; (c) and (g) Shear force at the base; (d) and (h) Bending moment at the base. (a) to (d) Beam in contact with water on one side; (e) to (h) beam in contact with water on two sides. Finite elements (Wet beam); Proposed method (Wet beam). Proposed method (Dry beam).

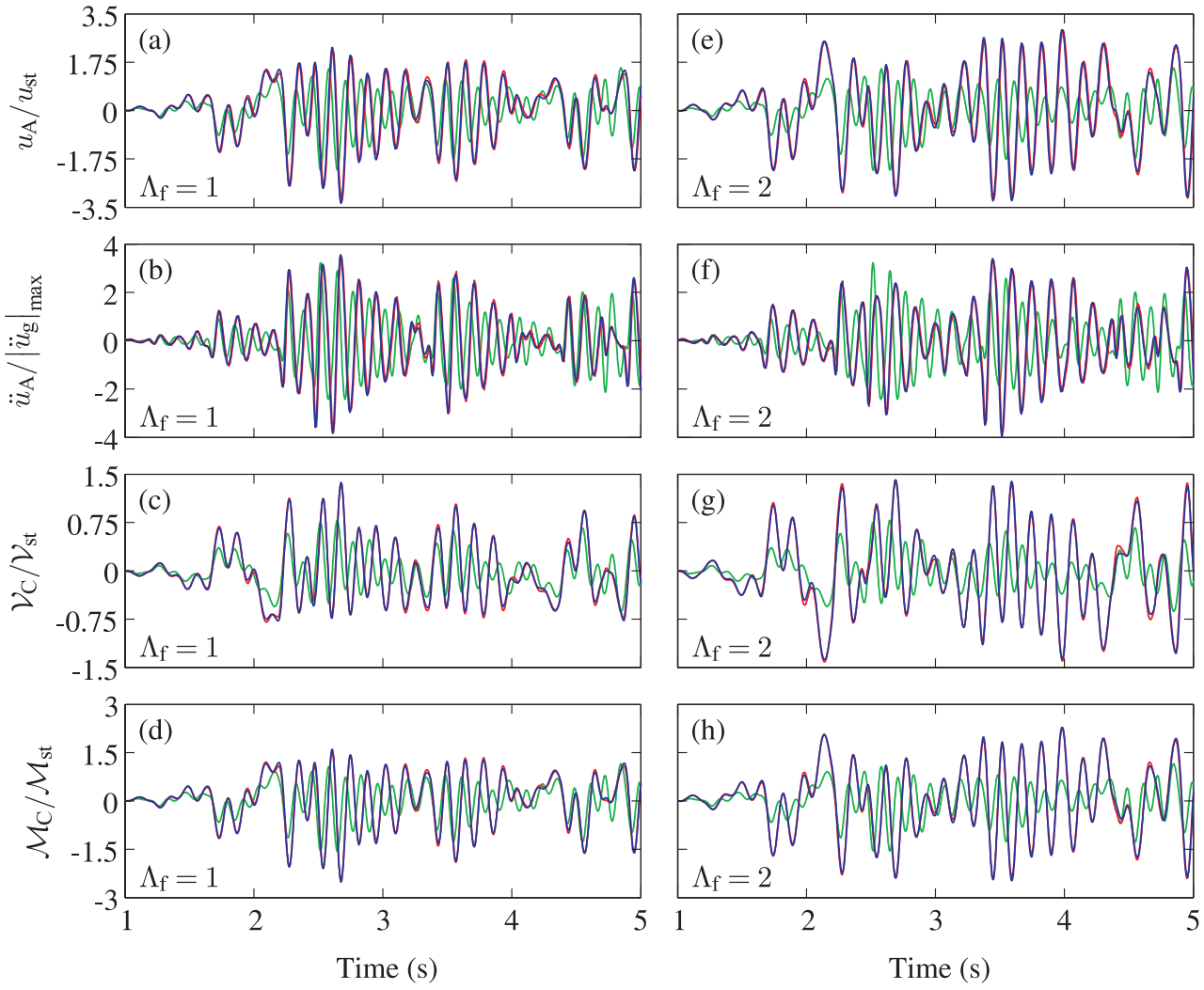

Figure 7. Time-history responses of the steel beam-fluid system - CF configuration: (a) and (e) Displacement at the top; (b) and (f) Acceleration at the top; (c) and (g) Shear force at the base; (d) and (h) Bending moment at the base. (a) to (d) Beam in contact with water on one side; (e) to (h) beam in contact with water on two sides. Finite elements (Wet beam); Proposed method (Wet beam). Proposed method (Dry beam).

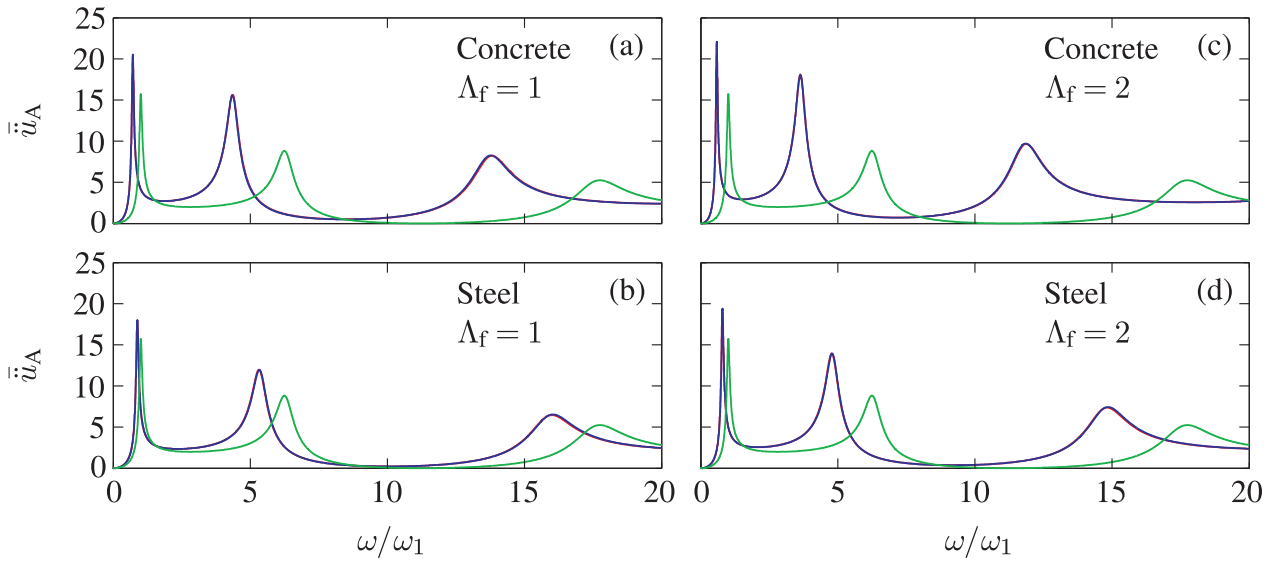

Figure 8. Frequency response curves for accelerations of concrete and steel beam-fluid systems - CF configuration: (a) Concrete beam in contact with water on one side; (b) Steel beam in contact with water on one side; (c) Concrete beam in contact with water on two sides; (d) Steel beam in contact with water on two sides. — Finite elements (Wet beam); — Proposed method (Wet beam); — Proposed method (Dry beam).

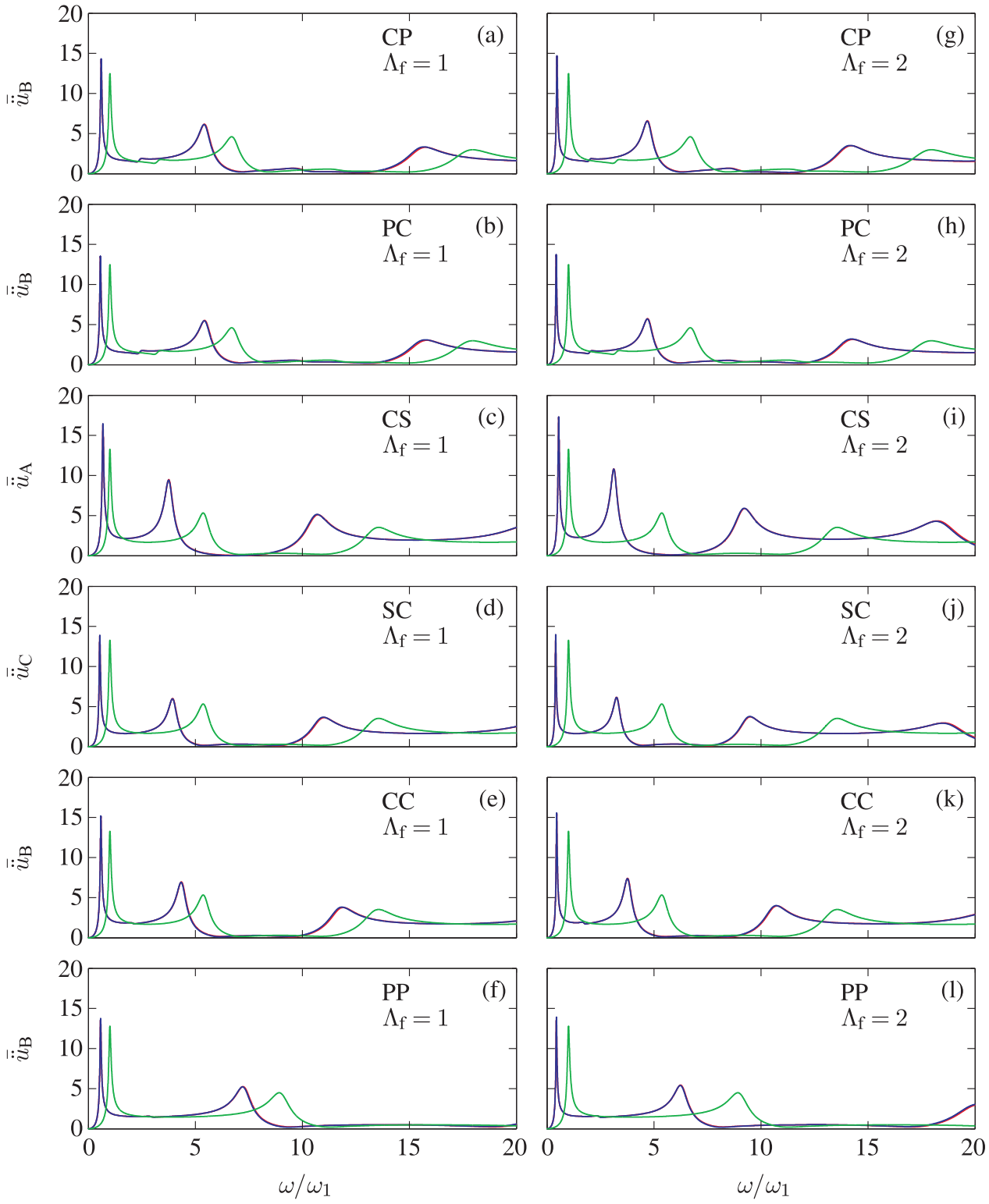

Figure 9. Frequency response curves for accelerations of concrete beam-fluid systems: (a) and (g) CP configuration; (b) and (h) PC configuration; (c) and (i) CS configuration; (d) and (j) SC configuration; (e) and (k) CC configuration; (f) and (l) PP configuration. (a) to (f) Beam in contact with water on one side; (g) to (l) Beam in contact with water on two sides. — Finite elements (Wet beam); — Proposed method (Wet beam); — Proposed analytical method (Dry beam).